

DESIGN OF A SAW OSCILLATOR AT A HARMONIC FREQUENCY

by



JOSEPH N. SFERRAZZA-PAPA, B.Eng.

A Thesis Submitted to the School of Graduate Studies  
in Partial Fulfilment of the Requirements  
for the Degree  
Master of Engineering

McMaster University  
Hamilton, Ontario

December 1981

DESIGN OF A SAW OSCILLATOR AT A HARMONIC FREQUENCY

MASTER OF ENGINEERING (1981)  
(Electrical Engineering)

McMaster University  
Hamilton, Ontario

TITLE: DESIGN OF A SAW OSCILLATOR AT A HARMONIC  
FREQUENCY

AUTHOR: Joseph N. Sferrazza Papa, B.Eng.  
(McMaster University)

SUPERVISOR: Professor C.K. Campbell

NUMBER OF PAGES: (vii), 100, Appendix 14

SCOPE AND CONTENTS: The resonator-type and delay line-type  
oscillators are discussed. The design  
and synthesis of a Surface Acoustic Wave  
Oscillator operating at a higher  
harmonic mode is presented.

## ABSTRACT

The use of harmonic mode SAW filters allows the fabrication of UHF oscillators with standard lithographic techniques. However, such devices previously required external filtering to select the desired harmonic. This in turn requires relatively high  $Q$  circuits with their associated alignment problems and phase sensitivity.

This thesis discusses a technique which permits harmonic operation without the external circuitry. By utilizing the theory of the end-fire array antenna a stepped-delay line has been fabricated at frequencies greater than 400 MHz using the fifth harmonic (i.e. fundamental at 80 MHz). The result is a packaged SAW oscillator which exhibited an output power of -15 dBm into a 50  $\Omega$  termination at a harmonic frequency of 404.3 MHz. Short term stability measurements made yield a short term stability of better than 1 part in  $10^9$  over a period of 1 sec.

## ACKNOWLEDGEMENTS

I wish to express my deep appreciation to my supervisor, Dr. C.K. Campbell for sharing with me his invaluable experience and knowledge of SAW devices and also for providing me with the best facilities possible to fabricate and test the SAW oscillator.

Thanks is also due to Mr. P.M. Naraine and Mr. Yanqin Ye for their stimulating discussions and advice.

I would like to thank Mr. Usik for maintaining and repairing the equipment used in these experiments.

Special appreciation is also appropriate for the time, effort and invaluable comments contributed by Dr. C.K. Campbell and Mr. P.M. Naraine in reviewing this thesis.

Finally, to Janet Arsenault go my sincere thanks for her excellent typing of the manuscript.

## TABLE OF CONTENTS

|  | <u>Page</u> |
|--|-------------|
| CHAPTER I INTRODUCTION   |             |
| 1.1 General  | 1           |
| 1.2 Scope of Thesis  | 2           |
| CHAPTER II A COMPARISON BETWEEN THE RESONATOR-TYPE AND<br>DELAY LINE-TYPE OSCILLATOR |             |
| 2.1 Introduction   | 4           |
| 2.2 Criteria for Oscillation   | 4           |
| 2.3 Mode Selection   | 13          |
| 2.4 Q-factor   | 21          |
| 2.5 SAW Oscillator Stability   |             |
| 2.5.1 Short Term Stability   | 28          |
| 2.5.2 Medium Term Stability  | 33          |
| 2.5.3 Long Term Stability  | 36          |
| 2.6 Circuit Complexity and Fabrication   | 37          |
| CHAPTER III DESIGN OF THE SAW DELAY LINES  |             |
| 3.1 Substrate Considerations   | 43          |
| 3.2 Design of Stepped-finger IDT Structure   |             |
| 3.2.1 Introduction   | 45          |
| 3.2.2 Theory of Stepped-finger Delay<br>Line   | 46          |
| 3.2.3 Equations and Calculations for<br>Stepped-finger Delay Lines                   | 53          |

TABLE OF CONTENTS (continued)

|  | <u>Page</u> |
|--|-------------|
| 3.3 Fabrication of the Saw Delay Line        |             |
| 3.3.1 Construction of the Delay Line Circuit | 60          |
| 3.3.2 Construction of SAW Oscillator Circuit | 62          |
| CHAPTER IV RESULTS                           |             |
| 4.1 Delay line Results                       | 69          |
| 4.2 SAW Oscillator Results                   | 86          |
| CHAPTER V CONCLUSIONS AND RECOMMENDATIONS    | 95          |
| REFERENCES                                   |             |
| APPENDIX A                                   | A-1         |
| APPENDIX B                                   | B-1         |
| APPENDIX C                                   | C-1         |

## LIST OF FIGURES.

| <u>Figure</u> |   | <u>Page</u> |
|---------------|---|-------------|
| 2.1           | Block diagram of the basic elements of the SAW oscillator.            | 5           |
| 2.2(a)        | Block diagram of the delay line-type oscillator.                      | 6           |
| (b)           | Block diagram of the resonator line-type oscillator.                  | 6           |
| 2.3           | Block diagram of the two-port resonator oscillator.                   | 7           |
| 2.4           | Finger spacing on delay line and resonator.                           | 8           |
| 2.5           | Analogous mass-spring oscillation system.                             | 10          |
| 2.6           | The comb of frequencies which can be supported by an oscillator.      | 15          |
| 2.7           | Mode selection by adjusting effective lengths.                        | 17          |
| 2.8           | Impedance model for the resonator structure.                          | 18          |
| 2.9           | Frequency response of the delay line and the resonator.               | 22          |
| 2.10          | SAW amplitude and phase response as a function of transducer spacing. | 24          |
| 2.11          | Measured noise performances of the delay line and the resonators.     | 34          |
| 2.12          | Temperature variations using SiO <sub>2</sub> overlay on ST-X quartz. | 35          |
| 3.1           | Material chart.   | 44          |
| 3.2           | 2-finger amplitude vs. metallization ratio.                           | 47          |
| 3.3           | 3-finger amplitude vs. metallization.                                 | 48          |
| 3.4           | 4-finger amplitude vs. metallization.                                 | 49          |



| <u>LIST OF FIGURES</u> (continued) |   | <u>Page</u> |
|------------------------------------|---|-------------|
| 3.5(a)                             | Two-finger structure.   | 50          |
| (b)                                | Stepped-finger structure.   | 50          |
| 3.6                                | Calculation of Null Percentage Bandwidth.                           | 58          |
| 3.7                                | Detailed schematic of the stepped-finger delay.                     | 61          |
| 3.8                                | Photograph of the cut delay line.                                   | 63          |
| 3.9(a)                             | Photograph of mounted delay line.                                   | 66          |
| (b)                                | Photograph of assembly of delay line and amplifier case.            | 66          |
| 3.10                               | Schematic Drawing of the SAW oscillator.                            | 67          |
| 3.11                               | Photograph of the complete SAW oscillator.                          | 68          |
| 4.1                                | Photograph of the HP Network Analyser 8505A.                        | 70          |
| 4.2(a)                             | Frequency response of mismatched delay line.                        | 71          |
| (b)                                | Bulk wave interference (expanded view).                             | 71          |
| 4.3(a)                             | Phase summation of ideal delay line at harmonic frequency.          | 74          |
| (b)                                | Phase summation of ideal delay line at unwanted harmonic frequency. | 74          |
| 4.4(a)                             | Phase error interference at harmonic frequency.                     | 75          |
| (b)                                | Phase error interference at an unwanted harmonic frequency.         | 75          |
| 4.5(a)                             | Photograph of frequency response of stepped-delay line.             | 76          |
| (b)                                | Photograph of bulk waves generated.                                 | 77          |
| 4.6(a)                             | Photograph of fundamental harmonic frequency.                       | 77          |
| (b)                                | Photograph of the 3rd harmonic frequency.                           | 77          |
| 4.7(a)                             | Photograph of the 7th harmonic frequency.                           | 78          |
| (b)                                | Photograph of the 9th harmonic frequency.                           | 78          |

| <u>LIST OF FIGURES (continued)</u>  | <u>Page</u> |
|---|-------------|
| 4.8(a) Photograph of desired harmonic mode.   | 79          |
| (b) Expanded view of the desired harmonic mode.   | 79          |
| 4.9(a) Photograph of the input impedance.   | 83          |
| (b) Photograph of the output impedance.   | 83          |
| 4.10(a) Photograph of the phase response.   | 84          |
| (b) Photograph of the group delay response.   | 84          |
| 4.11 Photograph of the 8555A spectrum analyzer.   | 87          |
| 4.12(a) Spread spectrum of closed loop oscillator<br>(illustrated amplifier).                               | 88          |
| (b) Spectrum of output oscillator.  | 88          |
| 4.13 Block diagram of set up for short term<br>stability measurements of SAW oscillators<br>in time domain. | 90          |
| 4.14 Photograph of the test set up for short term<br>stability measurements.                                | 91          |
| C-1 Electrical field diagram of unbalanced<br>connection.   | C-4         |
| C-2 Electrical field diagram of balanced<br>connection.   | C-6         |

LIST OF TABLES

|   | <u>Page</u> |
|---|-------------|
| Table I Description of the various Q's in a SAW resonator.                      | 27          |
| Table II Variation of operating frequency due to variations of metal thickness. | 40          |
| Table III Amplifier/directional coupler specifications.                         | 64          |
| Table IV Short term stability results for a 5th harmonic SAW oscillator.        | 94          |

LIST OF SYMBOLS USED

|                    |   |
|--------------------|---|
| A                  | attenuation due to bulk-scattering loss at grating edges. |
| a                  | beam width, normalized to wavelengths                     |
| $C_{T_1}, C_{T_2}$ | input/output capacitance                                  |
| $C_{FF}$           | static capacitance  |
| d                  | amount segment shifts in stepped-finger design.           |
| $f_0$              | fundamental frequency                                     |
| $f_1$              | operation frequency at $h^{\text{th}}$ harmonic           |
| h                  | harmonic used   |
| $L_1, L_2$         | length of input and output transducer                     |
| $L_{\text{eff}}$   | effective length of the cavity                            |
| n                  | number of half wavelengths in the effective cavity length |
| $N_1, N_2$         | number of finger pairs                                    |
| $Q_L$              | loaded Q  |
| $Q_m$              | material Q  |
| $Q_d$              | diffraction Q   |
| $Q_r$              | radiation Q   |
| R                  | reflection coefficient at grating reflectors              |
| T                  | transmission coefficient of the grating reflectors        |
| W                  | aperture  |
| $W_s$              | shifted finger aperture                                   |

LIST OF SYMBOLS USED (continued)

|             |   |
|-------------|---|
| X           | width of the Al finger.                           |
| y           | space between transducers                         |
| $ z_{11} $  | input impedance                                   |
| $\alpha$    | attenuation constant                              |
| $\beta$     | lossless propagation constant of the surface wave |
| $\lambda$   | wavelength  |
| $\lambda_0$ | fundamental wavelength                            |
| n           | metalization ratio                                |

## CHAPTER I

### INTRODUCTION

#### 1.1 General

The surface acoustic wave (SAW) oscillator is fundamentally a Rayleigh wave, which carries vibrational energy parallel to the surface of the solid. This type of oscillator should be contrasted with the conventional bulk quartz standing wave resonator used for oscillator control. The oscillator functions as follows, a wave is launched on a delay line, received at the other end, amplified and returned to the input of the delay line. The SAW oscillator is a multimode device and mode selection must be built into the loop for stable single mode operation.

High-Q quartz crystal resonators are used to stabilize the frequency of oscillator circuits. The most common used quartz crystal is the AT-cut which supports a highly temperature-stable bulk shear wave motion. Such oscillators pose certain disadvantages which leads to further developing the SAW oscillators. First, they are frequency limited to  $f_0 = 25$  MHz, hence one must use multipliers to operate at higher frequencies. Secondly, they are bulk, requiring careful mounting procedures and relatively fragile. Thirdly, since they are highly stable

source, they cannot be readily frequency-modulated, hence limited in their application as transmitters.

SAW oscillators, operating at the fundamental mode have been developed for beyond the range of modern bulk mode crystal oscillators. They are more rugged, use planar and integrated circuit techniques and in recent literature have proven their ability for frequency-modulating signals in the VHF/UHF range.

The stability of the SAW oscillator lies between that of the L.C. oscillator and the bulk quartz resonator. The frequency stability that can be achieved relates to the  $Q$  that can be achieved by the feedback loop by the oscillator. This thesis will discuss two types of feedback loop presently being used, they are the delay-line type and the resonator-type. The stability is defined in the time domain and a discussion is included on stability in the frequency domain.

## 1.2 Scope of Thesis

As mentioned above, there exist two types of SAW oscillators. This thesis intends to discuss the results of a comparative study of SAW delay line and resonator oscillators. Included are a number of factors, such as mode selection, achievable  $Q$ -factor, short term stability (noise), medium term stability (temperature), long term drifting (aging); circuit complexity and ease of device fabrication.

The thesis also includes an experimental study of a SAW oscillator built within the framework and capabilities of the SAW device fabrication laboratory at McMaster University. SAW devices can be made with fundamental frequencies below 200 MHz using photolithographic techniques. This upper limit is set by the resolution of the existing photoreductions lens (200 lines pair/mm) and the resolution in the limitations in the photoresist process.

The solution to the problem of operating the SAW device in the 200 MHz - 1 GHz range is to simply operate the device at a higher harmonic frequency which is in the 200 MHz - 1 GHz range, while the fundamental frequency is below 200 MHz, which allows one to use the photolithographic techniques available. Research conducted by P. Naraine, C.K. Campbell and Y. Ye [39], have developed a new transducer called the "stepped-finger" transducer, which efficiently generates the higher harmonic mode while filtering the mode from the undesired harmonics, which are simultaneously generated. The author intends to illustrate that a SAW oscillator operating at any of the harmonic frequencies has the same efficiency as a SAW oscillator operating at a fundamental mode. The main advantage being that a higher frequency range can be obtained with the stepped-finger delay line.



## CHAPTER II

### A COMPARISON BETWEEN THE RESONATOR-TYPE AND THE DELAY LINE-TYPE OSCILLATOR

#### 2.1 Introduction

A surface acoustic wave (SAW) oscillator consists of three individual elements. These elements are the phase shifter, the amplifier and the feedback element (the SAW device). As shown in Figure 2.1 the feedback element can consist of two different types of SAW devices; the delay line-type and the resonator-type as shown in Figure 2.2. The resonator shown in Figure 2.2(b) is referred to as the one-port structure, but a more advanced device is the two-port resonator which is a combination of the delay line and the one-port resonator as shown in Figure 2.3. The frequency of operation is proportional to the finger spacing in both the resonators and the delay lines (see Figure 2.4).

#### 2.2 Criteria for Oscillation

Why oscillation occurs in SAW oscillators can be explained using a mechanical analogy. It is known that a propagating Rayleigh wave travels across the surface of a piezoelectric crystal [1], causing a complex mixture of shear and longitudinal stress motions held together by the

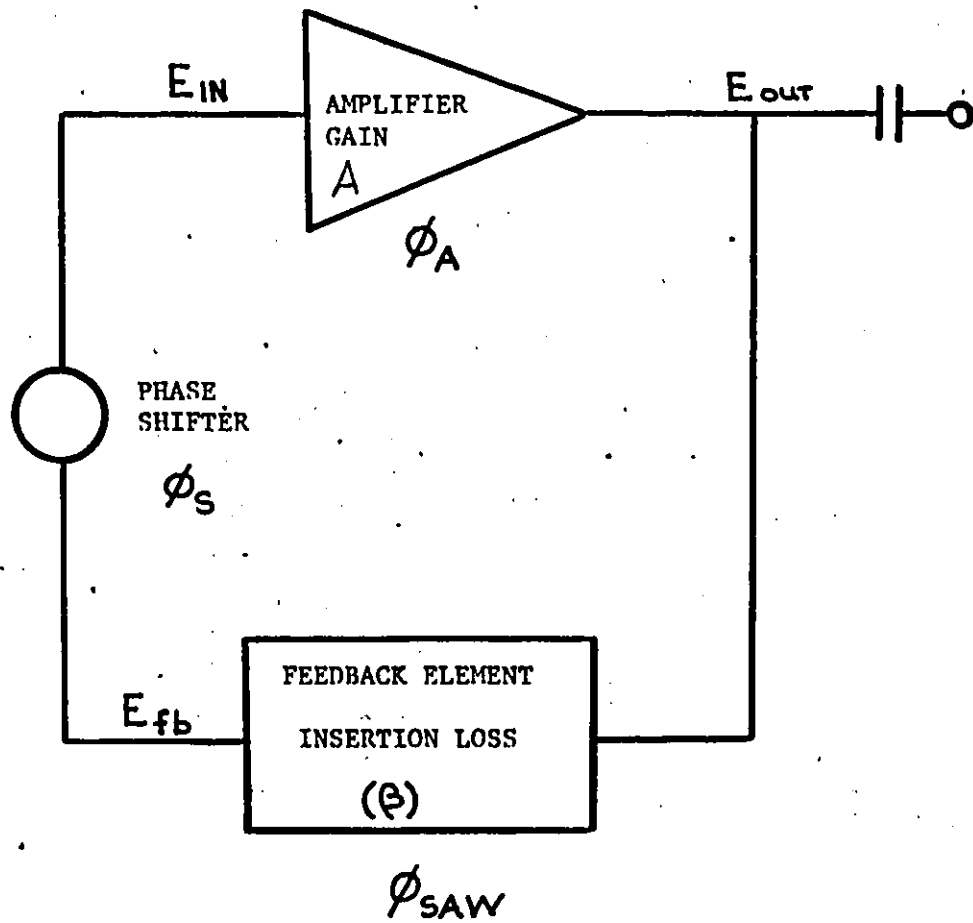
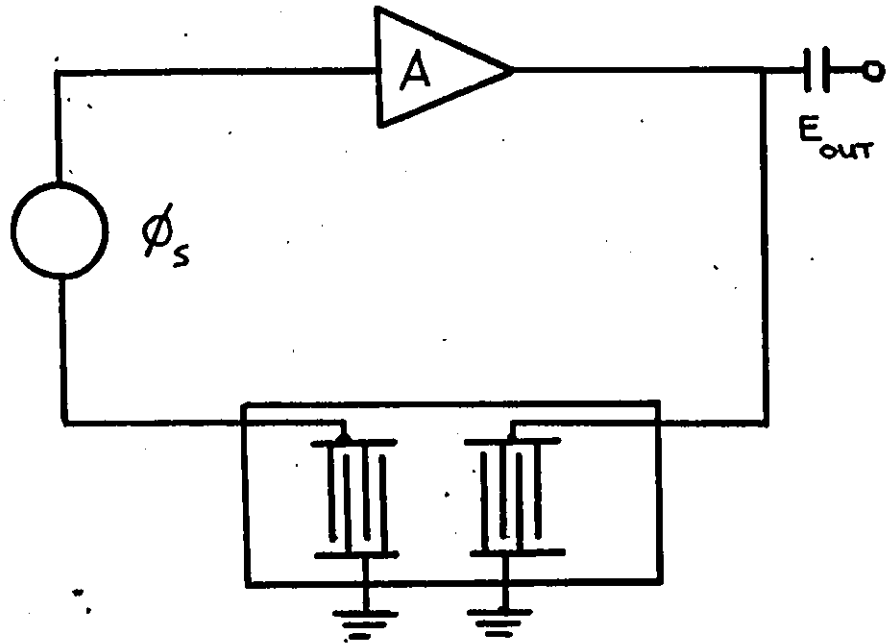
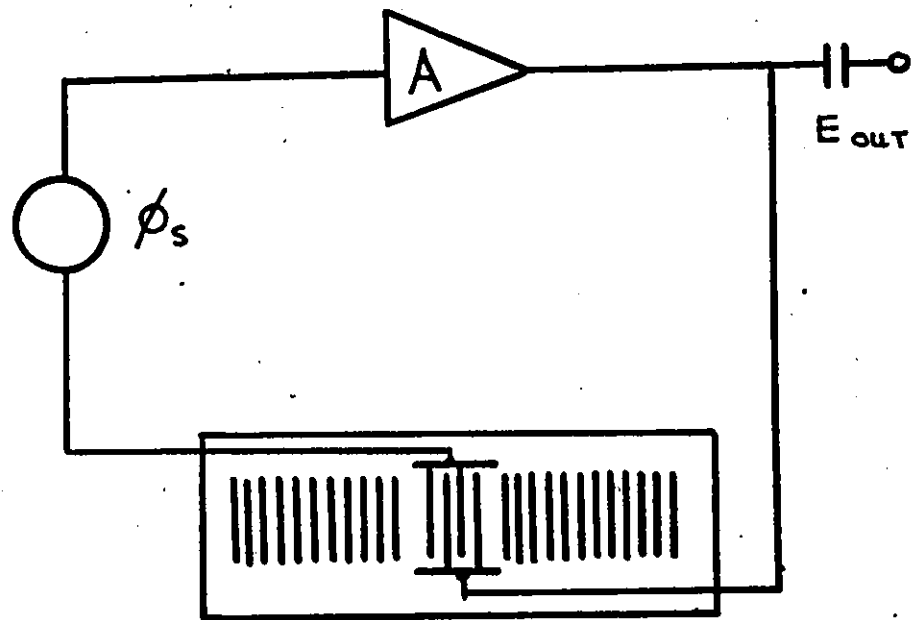


Figure 2.1

Block diagram of the basic elements of the SAW oscillator.



(a)



(b)

Figure 2.2(a) Block diagram of the delay line-type oscillator.

(b) Block diagram of the resonator line-type oscillator.

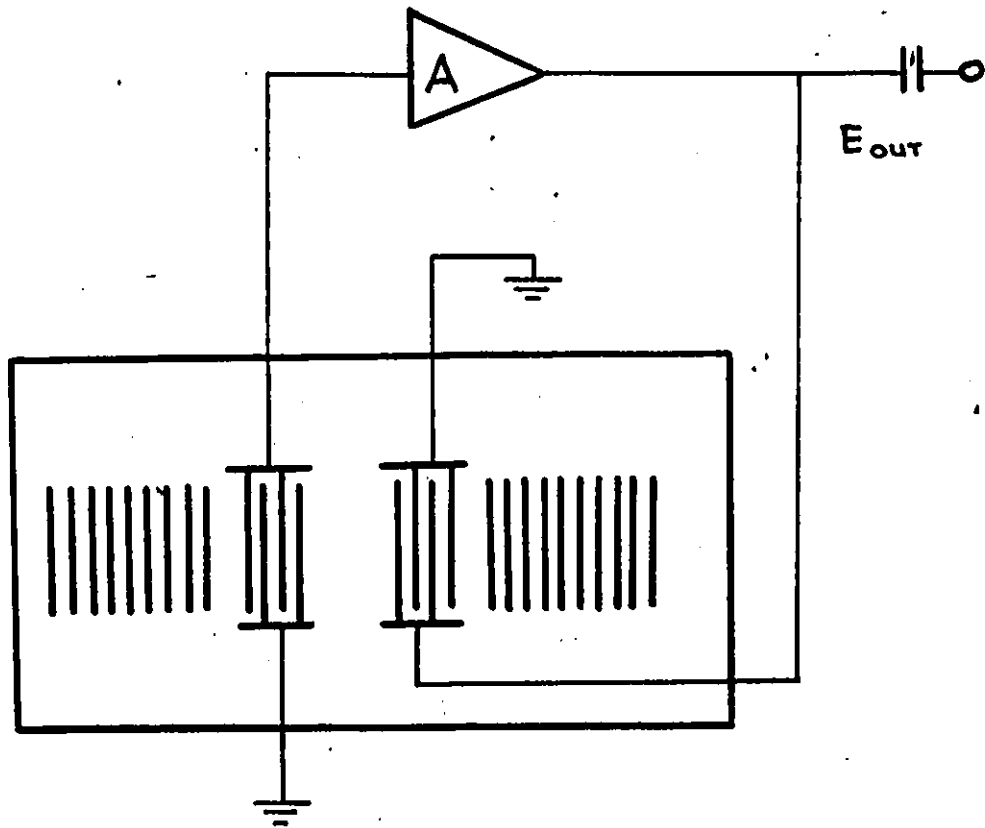
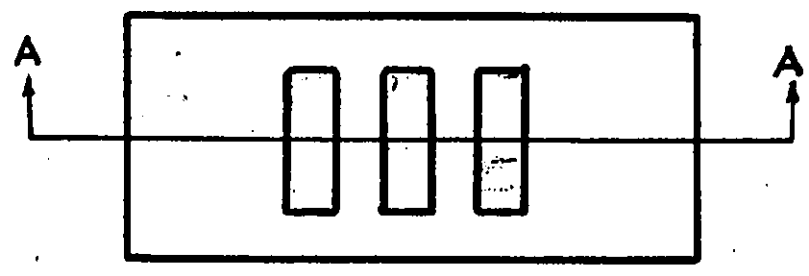
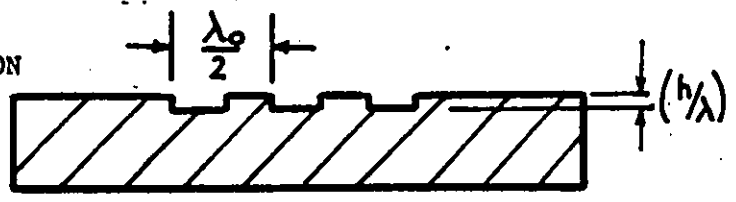


Figure 2.3 Block diagram of the two-port resonator oscillator.

TOP VIEW

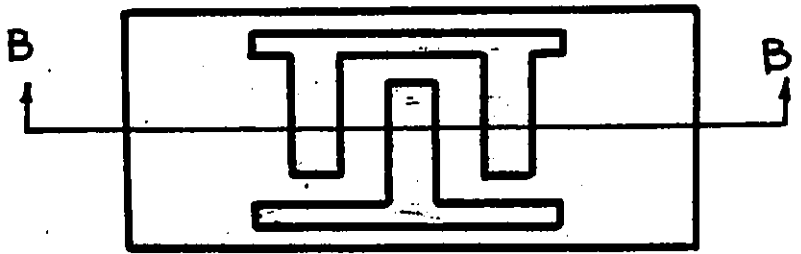


CROSS SECTION

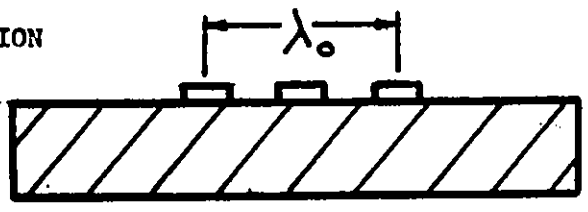


(a)

TOP VIEW



CROSS SECTION



(b)

Figure 2.4 Finger spacing on (a) delay line and (b) resonator.

presence of a stress free boundary condition. The stress motions extend only a few wavelengths into the crystal [9]. This interaction of the shear and longitudinal forces is the physical factor which maintains oscillation. This free oscillating system is analogous to the mechanical system of a mass spring action, where the displacement of the mass oscillates due to the frictionless surface and the spring action as illustrated in Figure 2.5.

Mathematically one can describe the conditions for oscillation to occur. These conditions are:

- i) The total gain around the closed loop must be unity,

$$A \cdot \beta = 1 \quad (2.2.1)$$

where

A + amplifier gain

$\beta$  + insertion loss of the SAW device.

- ii) The total phase shift about the closed loop must be an integer number of  $2\pi$  radians. From Figure 2.1 the total phase around the closed loop is,

$$\phi_A + \phi_{SAW} + \phi_S = 2\pi n \quad (2.2.2)$$

where  $\phi_A$ ,  $\phi_{SAW}$  and  $\phi_S$  are the phases of the amplifier, SAW device and the phase shifter, respectively.

Defining  $\phi_e$ , the electrical shift as,

$$\phi_e = \phi_A + \phi_S \quad (2.2.3)$$

where

$$\phi_e < 2\pi \text{ radians}$$

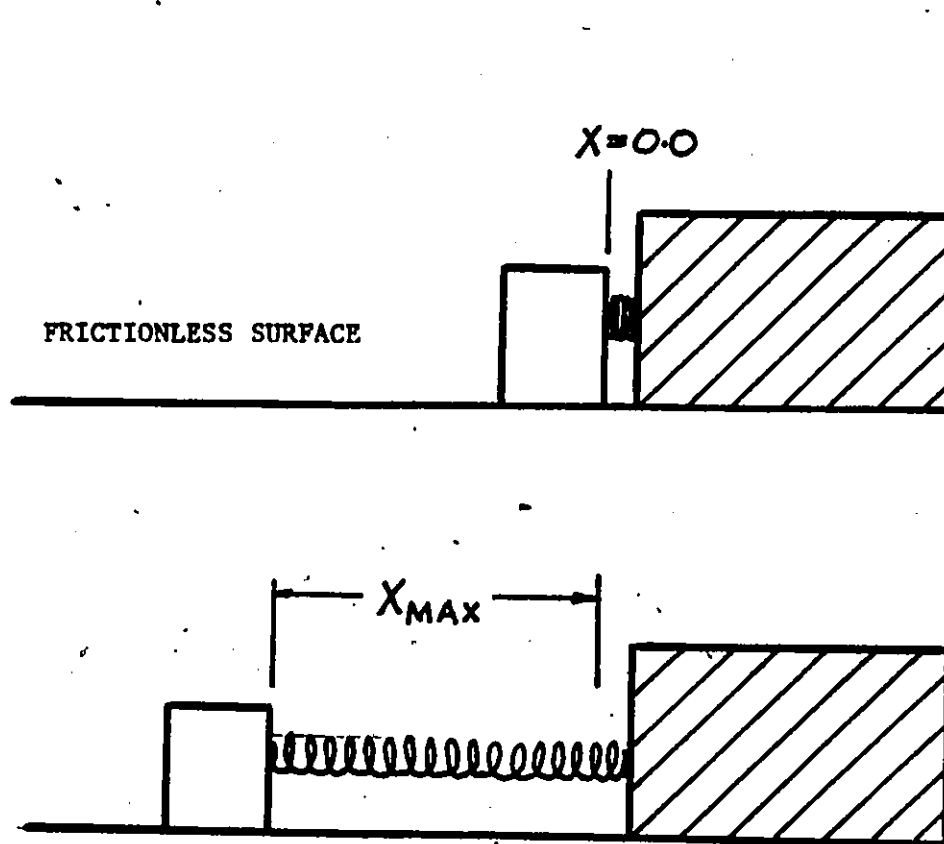


Figure 2.5 Analogous mass-spring oscillation system.

therefore

$$\phi_{\text{SAW}} + \phi_e = 2\pi n \quad (2.2.4)$$

The gain and phase constraints can be examined from a feedback control systems point of view, [2] and from the loop-phase condition, [3], respectively. From Figure 2.1 the first constraint for oscillation can be derived as follows,

$$E_{\text{in}} = E_{\text{fb}} \quad (2.2.5)$$

$$E_{\text{fb}} = \beta E_{\text{out}} \quad (2.2.6)$$

$$E_{\text{out}} = A E_{\text{in}} \quad (2.2.7)$$

substituting (2.2.6) and (2.2.7) into (2.2.5)

$$E_{\text{in}} = \beta A E_{\text{in}} \quad (2.2.8)$$

which reduces to

$$(1 - \beta A) E_{\text{in}} = 0$$

$$1 - \beta A = 0$$

therefore

$$\beta A = 1 \quad (2.2.9)$$

as stated in (2.2.1).

In justifying the phase constraint, we define  $\phi_N$  as the phase shift around the feedback loop, which contains  $N$  wavelengths. The value of  $N$  must be an integer by the loop-phase shift condition, hence

$$\phi_N = 2\pi N \quad (2.2.10)$$

Considering a delay line structure, the parameters involved are: the effective delay line length  $l_d$ ; the delay time,  $\tau$ ;



the phase shift through the delay line  $\phi_d$ ; the velocity of the surface wave  $v_s$ ; and the number of wavelengths in the delay line,  $N_d$ .

From (2.2.10) the phase in the delay line can be expressed as

$$\phi_d = 2\pi N_d \quad (2.2.11)$$

however  $l_d$  is defined as

$$l_d = N_d \lambda \quad (2.2.12)$$

the velocity of the SAW is given as

$$v_s = \frac{l_d}{\tau} \quad (2.2.13)$$

and the center frequency is defined as

$$f = \frac{v_s}{\lambda} \quad (2.2.14)$$

substituting for  $\lambda$  from (2.2.12)

$$f = \frac{v_s}{\left(\frac{l_d}{N_d}\right)} \quad (2.2.15)$$

multiplying by  $2\pi$

$$2\pi f = 2\pi \frac{v_s}{l_d} \times N_d$$

therefore

$$\omega = 2\pi N_d \left(\frac{v_s}{l_d}\right) \quad (2.2.16)$$

substituting for  $\phi_d$  from (2.2.11)

$$\omega = \phi_d \left( \frac{v_s}{l_d} \right)$$

therefore

$$\phi_d = \frac{\omega l_d}{v_s} = 2\pi N_d \quad (2.2.17)$$

Equation (2.2.10) can be expressed as

$$\phi_N = \phi_d + \phi_e = 2\pi N \quad (2.2.18)$$

substituting for  $\phi_d$  from (2.2.17) and for  $\phi_N$  from (2.2.10)

$$\frac{\omega l_d}{v_s} + \phi_e = 2\pi N \quad (2.2.19)$$

Equation (2.2.19) illustrates how the parameters of the SAW structure must satisfy the phase condition, but it poses a problem in mode selection. In most cases,  $\phi_d$  is much larger than  $\phi_e$ , hence the oscillation can occur at a comb of frequencies.

### 2.3 Mode Selection

The comb of frequencies results from the phase delay of the SAW being larger than the electrical circuit delay, i.e.;

$$\frac{\omega l_d}{v_s} \gg \phi_e$$

hence (2.2.19) reduces to [4]

$$\frac{\omega l_d}{v_s} = 2\pi N \quad (2.3.1)$$

$$\omega = \frac{2\pi N v_s}{l_d}$$

therefore

$$f = N \frac{v_s}{l_d} \quad (2.3.2)$$

Recall that the time delay  $\tau$  is defined as

$$\tau = \frac{l_d}{v_s} \quad (2.3.3)$$

Substituting (2.3.3) into (2.3.2) results in a comb of frequencies appearing at any integer value of  $N$  [5],

$$f = \frac{N}{\tau} \quad (2.3.4)$$

The specific mode for a delay line structure is selected by properly arranging the interdigital transducers (IDT) at the transmitting and receiving ends. The IDT has a normal response of the form [6]

$$H(f) = \left(\frac{\sin X}{X}\right)^2 \quad (2.3.5)$$

where

$$X = \frac{N\pi(\omega - \omega_0)}{\omega_0} \quad (2.3.6)$$

and  $N$  is the number of interdigital periods [7]. Figure 2.6

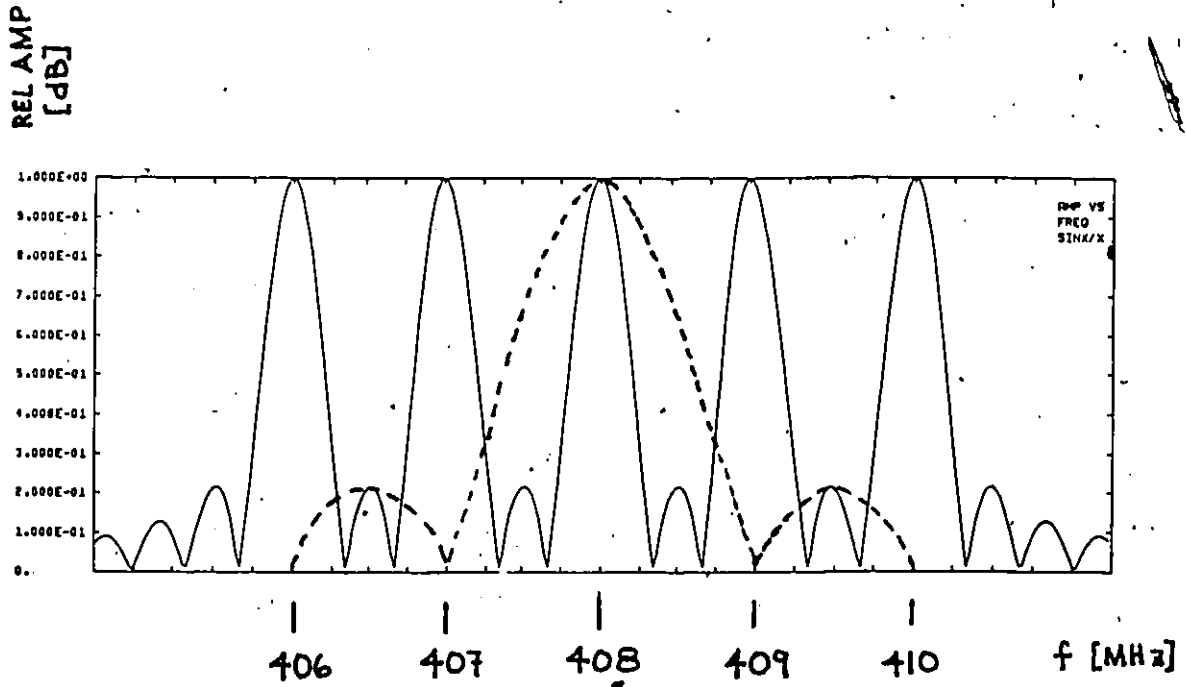


Figure 2.6. The solid curve illustrates the comb of frequencies which can be supported by an oscillator. The dashed curve illustrates the required frequency to be selected.

illustrates the comb of frequencies with the null bandwidths of each response given by

$$BW = \frac{2\omega_0}{N} \quad (2.3.7)$$

Since the mode separation is

$$\Delta\omega = \frac{2\pi}{\tau} \quad (2.3.8)$$

it follows that the IDT bandwidth can be made narrow enough to select just one mode, if the IDT transducer length is made equal to the propagation length,  $l_d$  [8], i.e.

$$l_d = N\lambda \quad (2.3.9)$$

as shown in Figure 2.7.

Mode selection in the SAW resonator is not considered a problem because of the nature of the resonator. A cavity structure is formed by reflecting an oscillating wave upon itself many times. The waves are launched from the IDT and propagate away from the IDT, into the grating reflectors. Coherent multiple reflections occur and a large standing wave is set up within the cavity. Basically, the cavity acts as a notch filter. All the energy will pass through it except at the resonant frequency. The resonator may be visualized as a large number of reflecting section,  $N_R$ . Each section consisting of a quarter wavelength strip of impedance  $Z_1$  and a quarter wavelength gap of impedance  $Z_0$ , see Figure 2.8.

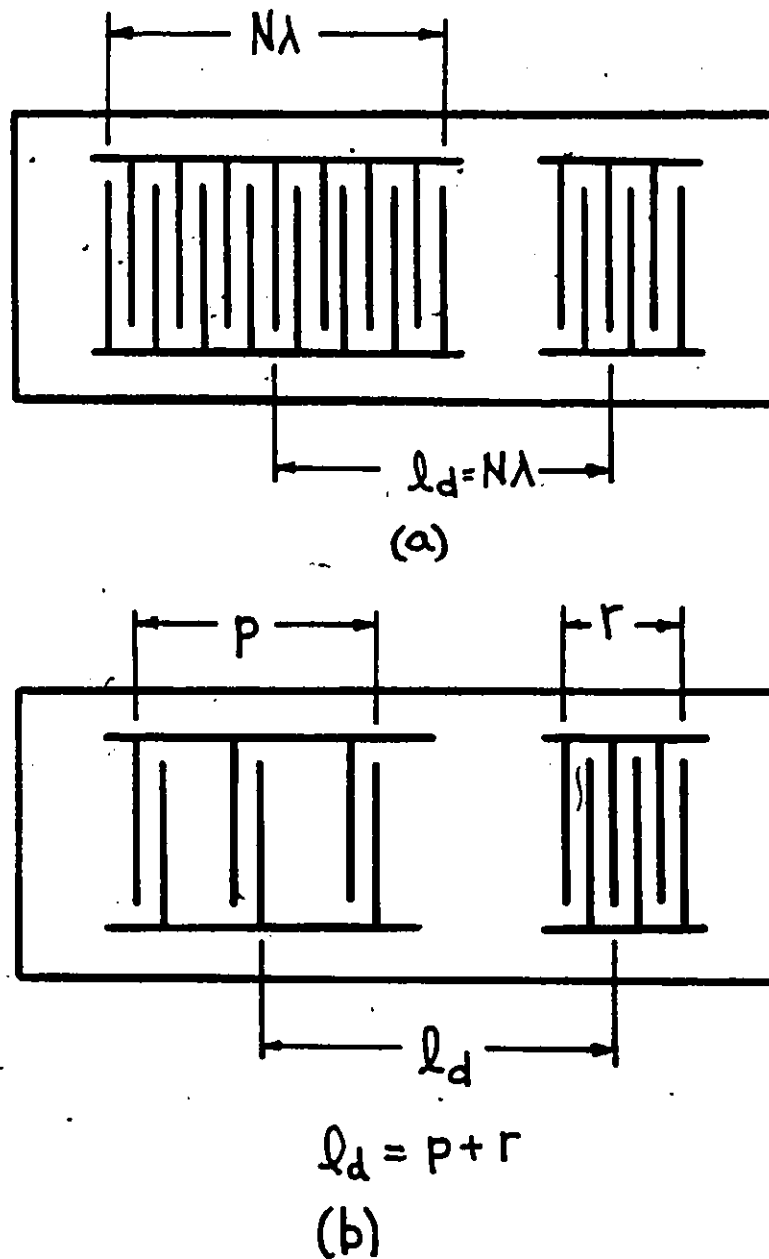


Figure 2.7 Mode selection:

- (a) the left hand side transducer performs the selection; the right hand side is for a very wide band response.
- (b) the combined response of two transducers performing the mode selection.

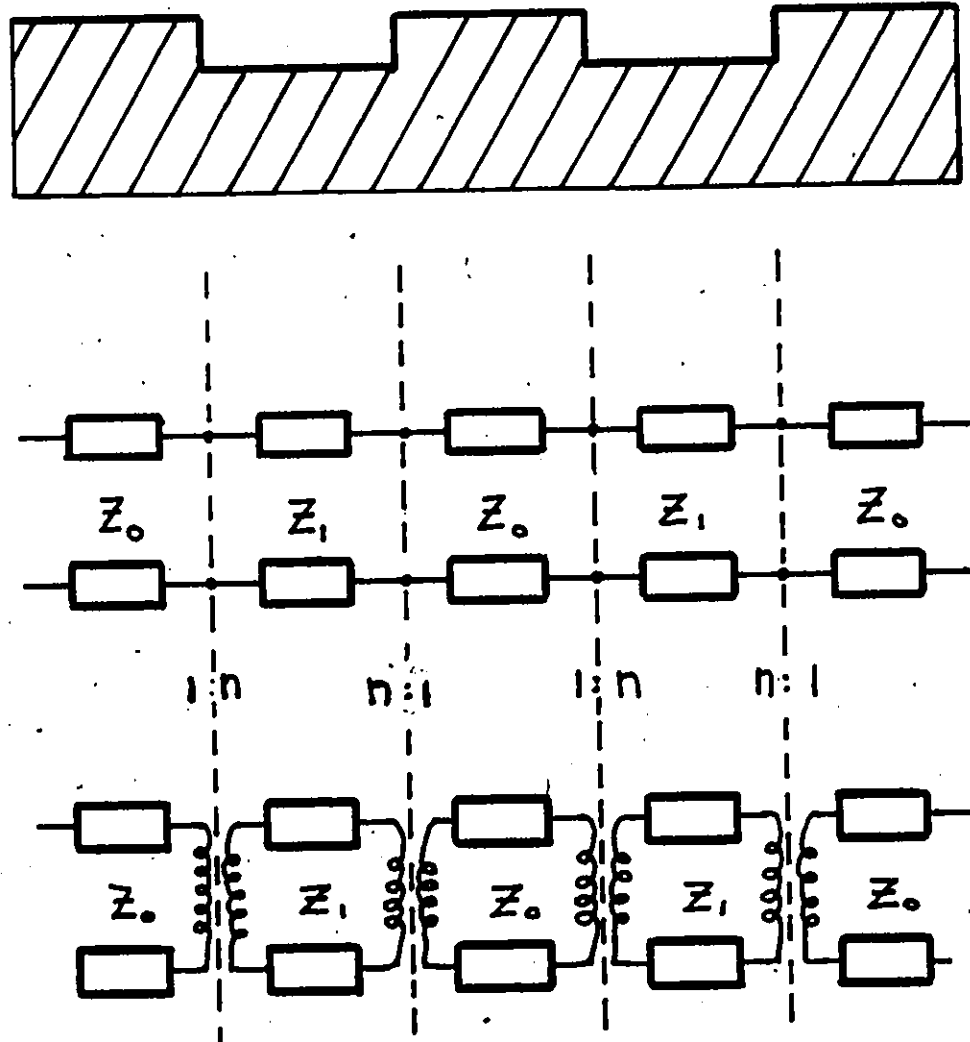


Figure 2.8 Impedance model for the resonator structure.

- (a) physical cross-section of the grooves.
- (b) electrical model with impedance mismatches, by Sittig and Coquin [34].
- (c) model by Oliner et al. [11] describing the array of grooves.

The impedance has no physical meaning and is only a means of characterizing the reflections from the edges. Because of the impedance discontinuity, each reflecting section contributes a small reflection of the wave as it propagates through the section.

The bandwidth is inversely proportional to the number of reflectors (or number of finger pairs). Typically, the resonator has 1000 to 2000 grooved reflectors and the IDT structures have 100 finger pairs. The bandwidth over which the surface waves are reflected and also over which the phase matching to unwanted bulk modes can occur, is much smaller than the IDT bandwidth. The coherent reflection of energy by the reflectors creates a narrow stopband in the overall passband. The depth of the stopband is related to the transmission coefficient  $T(f)$  and the reflection coefficient  $R(f)$  of the reflectors at a given frequency,  $f$ . Thus  $r$ , the reflection coefficient per step, is related as (from transmission line theory [10]),

$$r = \frac{Z_1 - Z_0}{Z_1 + Z_0} \quad (2.3.10)$$

In the case of a cascaded number of steps the model changes [11] the  $r$  value to

$$r = \frac{n^2 - 1}{n^2 + 1} = n - 1 \quad (2.3.11)$$

where  $n$  is an effective transformer ratio.



In combining the two models above together, the reflection coefficient at the center frequency becomes [10]

$$|R(f)| = \frac{|(z_1/z_0)^{2N} - 1|}{|(z_1/z_0)^{2N} + 1|} \quad (2.3.12)$$

where  $N$  is the number of grooves. From transmission line theory the transmission coefficient can be calculated from

$$|R(f)|^2 + |T(f)|^2 = 1 \quad (2.3.13)$$

therefore

$$|T(f)|^2 = 1 - |R(f)|^2$$

$$|T(f)|^2 = 1 - \frac{|(z_1/z_0)^{2N} - 1|^2}{|(z_1/z_0)^{2N} + 1|^2} \quad (2.3.14)$$

let

$$z = z_1/z_0$$

and

$$A = 2N$$

Hence (2.3.14) reduces to

$$|T(f)|^2 = 1 - \frac{|z^A - 1|^2}{|z^A + 1|^2} \quad (2.3.15)$$

$$|T(f)|^2 = \frac{|z^A + 1|^2}{|z^A + 1|^2} + \frac{|z^A - 1|^2}{|z^A + 1|^2}$$

$$|T(f)|^2 = \frac{(z^{2A} + 2z^A + 1) + (z^{2A} - 2z^A + 1)}{|z^A + 1|^2}$$

therefore equation (2.3.14) reduces to

$$|T(f)| = \frac{2(z_1/z_0)^N}{(z_1/z_0)^{2N} + 1} \quad (2.3.16)$$

Finally, the separation between the cavity and the reflectors must be an integer number of half wavelengths for the structure to resonate.

#### 2.4 Q-factor

The frequency response of the delay line and resonator are illustrated in Figure 2.9. The resonator has a lower insertion loss and a higher Q value as a result of the sharpness of the passband. Typically the delay line has a Q value of  $Q \approx 500-1,500$ , whereas the resonators (both one-port and two-port) have Q's in the range  $Q \approx 2,000-30,000$  [12].

The definition of the Q-factor in the microwave field is

$$Q = \omega_0 \times \left( \frac{\text{energy stored}}{\text{power loss}} \right) \quad (2.4.1)$$

The term Q factor has no physical meaning when applied to a SAW delay line, since such a delay line does not involve energy storage.

The Q for a delay line is usually expressed in terms of the phase slope, as will be shown below, since the phase

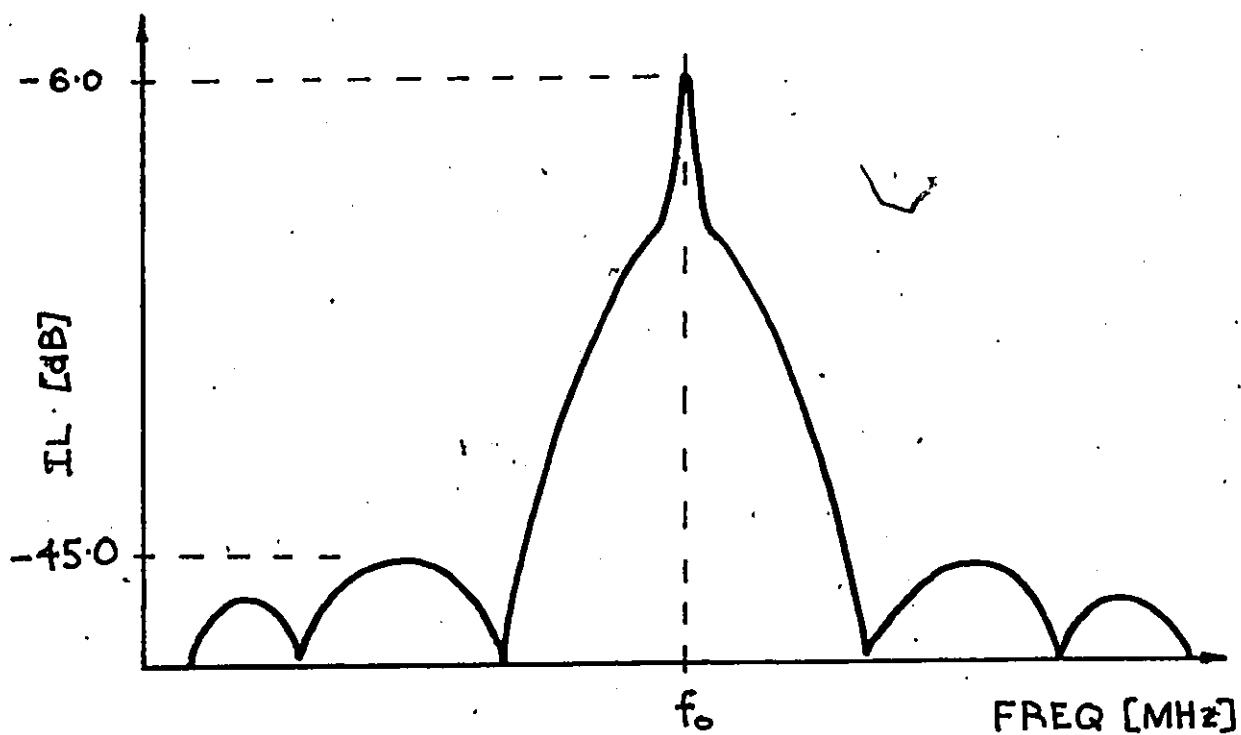
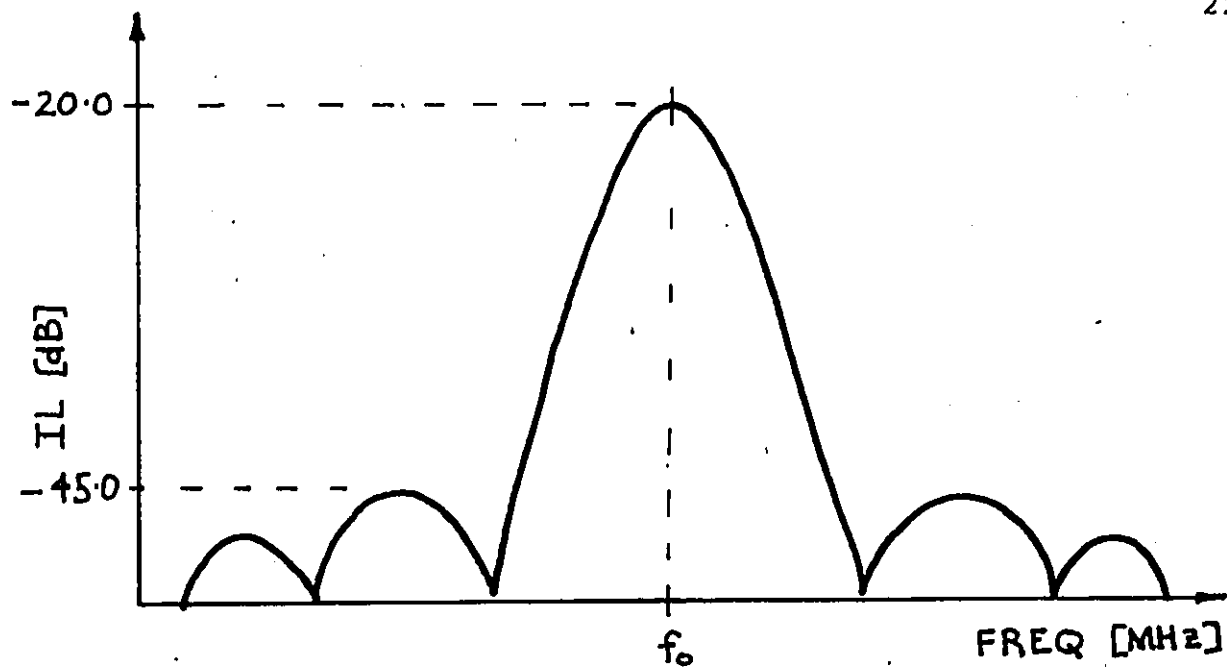


Figure 2.9 Frequency response of the (a) delay line and (b) resonator.

slope of the delay line is designed for a desired FM bandwidth. For very narrow bandwidths the phase slope is made to be very steep (see Figure 2.10). Hence the oscillator stability will approach that of the delay line and would increase the overall stability [2].

In order to establish a definition of the Q-factor for the delay lines, the phase slope can be compared to that of the phase slope of a LC circuit at the resonant frequency. Hence,

$$\theta = \tan^{-1} \left( \frac{\frac{1}{\omega C} - \omega L}{R} \right) \quad (2.4.2)$$

The phase slope is defined as

$$\frac{d\theta}{d\omega}$$

At the resonant frequency,  $\omega = \omega_0$

$$\omega_0 L = \frac{1}{\omega_0 C} \quad )$$

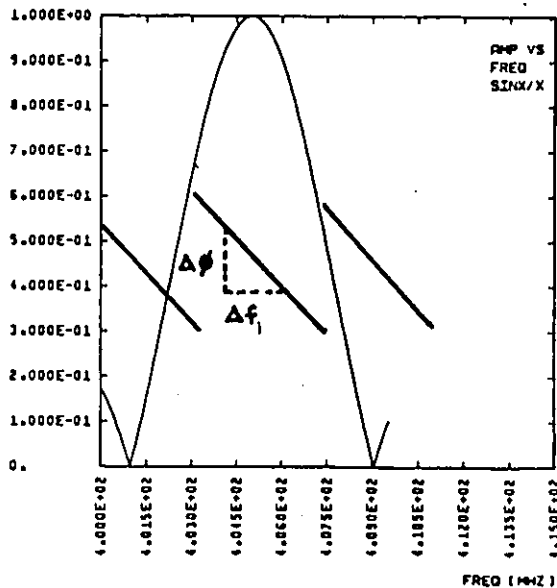
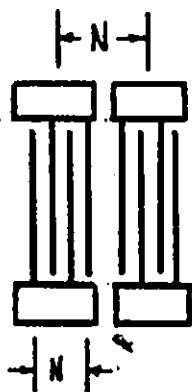
thus

$$\left. \frac{d\theta}{d\omega} \right|_{\omega=\omega_0} = - \frac{2\omega_0 L}{\omega_0 R} \quad (2.4.3)$$

but from the parallel resonant circuit

$$Q = \frac{\omega_0 L}{R} \quad (2.4.4)$$

Thus from equation (2.4.3)



Note:  $\Delta f_1 > \Delta f_2$

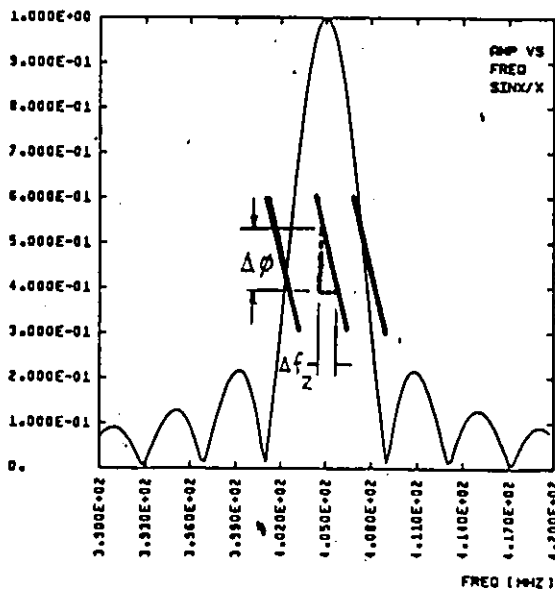
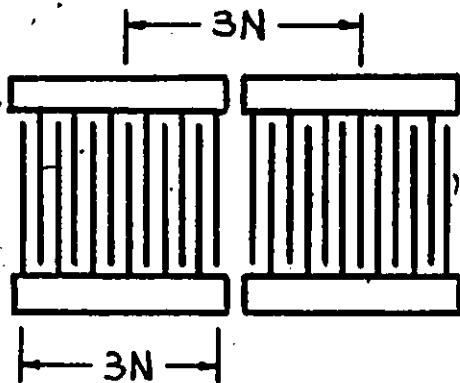


Figure 2.10 SAW amplitude and phase response as a function of transducer spacing.

$$\left. \frac{d\theta}{d\omega} \right|_{\omega=\omega_0} = -\frac{2Q}{\omega_0} \quad (2.4.5)$$

The phase slope of a non-dispersive delay line of delay  $\tau_d$  is given by [13]

$$\frac{d\theta}{d\omega} = -\tau_d \quad (2.4.6)$$

Hence the  $Q$  of the delay line based on the phase slope is given by substituting (2.4.6) into (2.4.5) and rearranging terms,

$$Q = \frac{\tau_d \omega_0}{2}$$

or

$$Q = \tau_d \pi f_0 \quad (2.4.7)$$

Further development of the  $Q$  as relating to the physical delay line parameters can be established. The phase slope of the delay line given in (2.4.6) can also be expressed in terms of the physical geometry of the delay line [14], where

$$\tau_d = \frac{N'}{f_0} \quad (2.4.8)$$

where  $N'$  (in units of wavelengths) is the number of wavelengths in the time delay. Hence (2.4.7) becomes,

$$Q = \pi N' \quad (2.4.9)$$

For example, a delay line has a time delay  $\tau_d = 0.25 \mu\text{sec}$ , (equations for calculation of these parameters can be found in reference [15]), with a center frequency of  $f_0 = 300 \text{ MHz}$ .

Thus, the calculated  $Q$  is:

$$\begin{aligned} N' &= \tau_d f_0 \\ &= (0.25 \text{ } \mu\text{sec}) \times (300 \text{ x MHz}) \end{aligned}$$

$$N' = 75 \lambda$$

$$Q = \pi N' = \pi (75\lambda)$$

Therefore

$$Q = 235$$

In the surface acoustic resonator, the  $Q$ -factor is determined from the various sources of losses associated with the cavity. In the case of a two-port resonator, as shown in Figure 2.3, various  $Q$ 's are listed in Table I [16]. Hence (2.4.10) can be used to calculate the loaded  $Q$  of the resonators,

$$\frac{1}{Q_L} = \frac{1}{Q_m} + \frac{1}{Q_d} + \frac{1}{Q_b} + \frac{1}{Q_r} \quad (2.4.10)$$

In the final analysis, even though the  $Q$  of the delay line is linear it is limited to an upper bound of 2000 because of fabrication problems, and mass loading due to a large number of finger pairs on the crystal. The resonator, though, can be constructed with  $Q$ 's in the range  $Q \approx 2000$ -20,000. The upper limit is determined by the material  $Q$ ,  $Q_m$ , which is in the neighbourhood of  $Q \approx 70,000$  [16]. But due to scattering losses into the bulk at the grating edges and the radiation losses at the grooves depths, this limit is still very much under investigation by Williamson [16]

TABLE I

Description of the various Q's in a SAW resonator.

| Notation          | Description  |
|-------------------|--|
| $Q_L \Rightarrow$ | loaded Q   |
| $Q_m \Rightarrow$ | material Q, $Q_m = \beta/2\alpha$ , associated with the propagation loss on the crystal's surface. |
| $Q_d \Rightarrow$ | diffraction Q, $Q_d = (a/\lambda)^2$ , from losses due to diffraction of the surface wave beam.    |
| $Q_b \Rightarrow$ | bulk scattering Q, $Q_b = \beta L_{eff}/2A$ , due to bulk wave radiation.                          |
| $Q_r \Rightarrow$ | radiation Q, $Q_r = n\pi/1-R^2$ , due to leakage through the imperfectly reflecting gratings.      |



where groove depths and number of grooves on the crystal, are being considered. The implication of implementing a SAW feedback element with a higher  $Q$  is to improve the short term stability of the oscillator.

## 2.5 SAW Oscillator Stability

It is convenient to divide the stability criteria of oscillators into three groups. Short term or spectral purity, medium term stability and long term stability aging. The short term stability (less than 1 sec) arises from electrical noise sources within the loop and from external sources such as vibration. The medium term stability (greater than 1 sec) is dominated by the variation of frequency with temperature and the long term (greater than 1 day) effects are caused by slow physical changes in the material of the device and the cleanliness of the crystal's surface [17].

### 2.5.1 Short Term Stability

There are two ways of characterizing the frequency stability of an oscillator. Analyses can be made in the time domain and in the frequency domain. The time domain analysis is based on the fractional frequency stability as a function of the measured period,  $T$ . The oscillator stability in the time domain is measured by evaluating the

Allan variance defined by  $\sigma_y^2(2, \tau)$

$$\sigma_y^2(t, \tau) = \left\langle \frac{(\bar{y}_{k+1} - \bar{y}_k)^2}{2} \right\rangle \quad (2.5.1)$$

where  $y_k$  is the fractional frequency averaged from  $t_k$  to  $t_{k+1}$  [18]. In the frequency domain the emphasis is on the calculation of the FM noise (phase noise). The conventional way of expressing FM noise is as a single sideband noise power spectrum [19]. This expression (equation 2.5.2) is based on work by Leeson [20]

$$\left( \frac{P_{SB}}{P_C} \right) = 10 \log_{10} \left[ \left( \frac{N^2 G F k T}{P_C} \right) \left( \frac{\omega_\alpha}{(\Delta\omega)^3 \tau^2} + \frac{1}{(\Delta\omega)^2 \tau^2} + 1 \right) \right] \quad (2.5.2)$$

where

$N$  → multiplication factor

$G$  → amplifier gain = SAW insertion loss

$kT$  → thermal energy

$F$  → oscillator power at amplifier output

$\tau$  → phase slope (group delay) of the SAW device

$\omega_\alpha$  → flicker frequency constant,  $\omega_\alpha = 5 \times 10^{-17}$  [21]

$\Delta\omega$  → offset or modulation frequency.

Equation (2.5.2) is not an exact expression, but gives a close approximation to the noise power spectrum [19].

The general method of analyzing short term stability in the frequency domain is to consider phase noise. The phase noise is expressed by the spectral density, script  $\mathcal{L}(f)$ ,

which is defined as

$$\text{Script } \mathcal{L}(f) = 10 \log_{10} \left[ \frac{\text{power density (one phase modulated sideband)}}{\text{carrier power}} \right] \quad (2.5.3)$$

or

$$\text{Script } \mathcal{L}(f) = \left( \frac{P_{\text{SB}}}{P_{\text{C}}} \right)_{\text{dB}} \quad (2.5.4)$$

From small angle modulation theory (2.5.4) reduces to

$$\text{Script } \mathcal{L}(f) = \frac{S_{\phi}(f)}{2} \quad (2.5.5)$$

(see Appendix A for detailed calculation involving (2.5.5)). Equation (2.5.2) has been found to be accurate to within a few dB [20]. The three terms in the right-hand parenthesis represent the thermal noise (loop amplifier noise, assume  $N = 1$ ),  $GFkT/P_{\text{C}}$ , the additive noise (group delay or phase slope in the noise power spectrum), is expressed by  $GFkT/P_{\text{C}} \cdot 1/\Delta\omega^2 \tau^2$ , and the flicker noise is  $GFkT/P_{\text{C}} \cdot \omega_{\text{a}}/\Delta\omega^3 \tau^2$ . The thermal noise is frequency dependent since it depends completely on the amplifier gain and the noise figure, as well as the kTB product. The phase slope term is due to the frequency modulation of the oscillator caused by phase noise in the amplifier. The flicker noise is related to the physical resonance mechanism in an oscillator [22]. This can result from noisy electronics such as the amplifier. The open loop  $f^{-1}$  close-to-carrier flicker phase noise

transforms to the  $f^{-3}$  flicker frequency noise in the closed loop system [23].

In the time domain the stability of an oscillator is characterized by statistical fluctuations about the mean frequency,  $f_0$ . The relationship between the Allan variance and the fractional frequency variation is given by (2.5.6) [19]

$$\frac{\Delta f}{f} = \sqrt{\sigma^2(N, \tau)} \quad (2.5.6)$$

where

$N$  + adjacent samples of averaged frequency

$\tau$  + the averaging time

Plots of  $(\sigma^2(N, \tau))^{1/2}$  vs  $\tau$  are commonly used to express the short term stability where  $\tau$  is usually defined as the interval [23]

$$0.001 \leq \tau \leq 1 \text{ sec}$$

The philosophy of the time domain measurements is that an oscillator of known stability is heterodyned with the oscillator under test. The changes in the period of the difference frequency indicates the instability of the test oscillator relative to the stable source oscillator. The following approximation can be used [24]

$$f = \frac{1}{\tau} \quad (2.5.7)$$

where  $\tau$  is the period (sec) which is from the oscillator

under test and which is read directly from the counter.

Differentiating,

$$df = -\frac{d\tau}{\tau^2} \quad (2.5.8)$$

Dividing both sides by  $f_0$

$$\frac{df}{f_0} = -\frac{d\tau}{\tau^2 f_0} \quad (2.5.9)$$

For small changes

$$\frac{\Delta f}{f_0} = -\frac{\Delta \tau}{\tau^2 f_0} \quad (2.5.10)$$

where

$\frac{\Delta f}{f_0}$  + the fractional frequency offset

$\Delta \tau$  + change in the period displayed on the counter

$\tau$  + period of the difference frequency

$f_0$  + operating frequency.

Investigators comparing short term stability of the resonator and delay line structures have reported results in both the time domain and in the the frequency domain. In both domains the resonator has generally yielded better short term stability results than the delay line structure. Experiments conducted by Parker [19] (considering FM noise measurements using (2.5.2)) showed that theoretically the ideal delay line has a better noise performance than the resonator, but the resonator can be fabricated closer to the

theory than the delay line. For both the resonator and delay line, the material propagation loss ultimately limits the noise performance of the SAW device. It may be shown that an ideal SAW delay line (see Appendix B for insertion loss calculations), has a close-in noise level about 3 dB lower than a perfect resonator.

For very narrow bandwidths or fixed frequency applications, the resonator-type oscillator will give the best noise performance (see Figure 2.11). For applications where tunability and linearity are important, the delay-line oscillator will give better performance.

### 2.5.2 Medium Term Stability

The medium-term stability of a SAW oscillator is determined by the temperature dependence of the SAW velocity on a given substrate. The best choice of material, to date, has been ST-X quartz, but substantially better temperature stability can be obtained with a  $\text{SiO}_2$  film overlay on YZ  $\text{LiTaO}_3$ . Parker and Shulz [26] reported this structure having the second-order temperature coefficient of delay (TCD) an order of magnitude smaller than that of ST-x quartz (see Figure 2.12). The use of a layer of  $\text{SiO}_2$  does not complicate the fabrication process. The  $\text{SiO}_2$  thickness must be controlled to within 0.1% [26], but trimming can easily be accomplished by ion etching. The layer can be sputtered

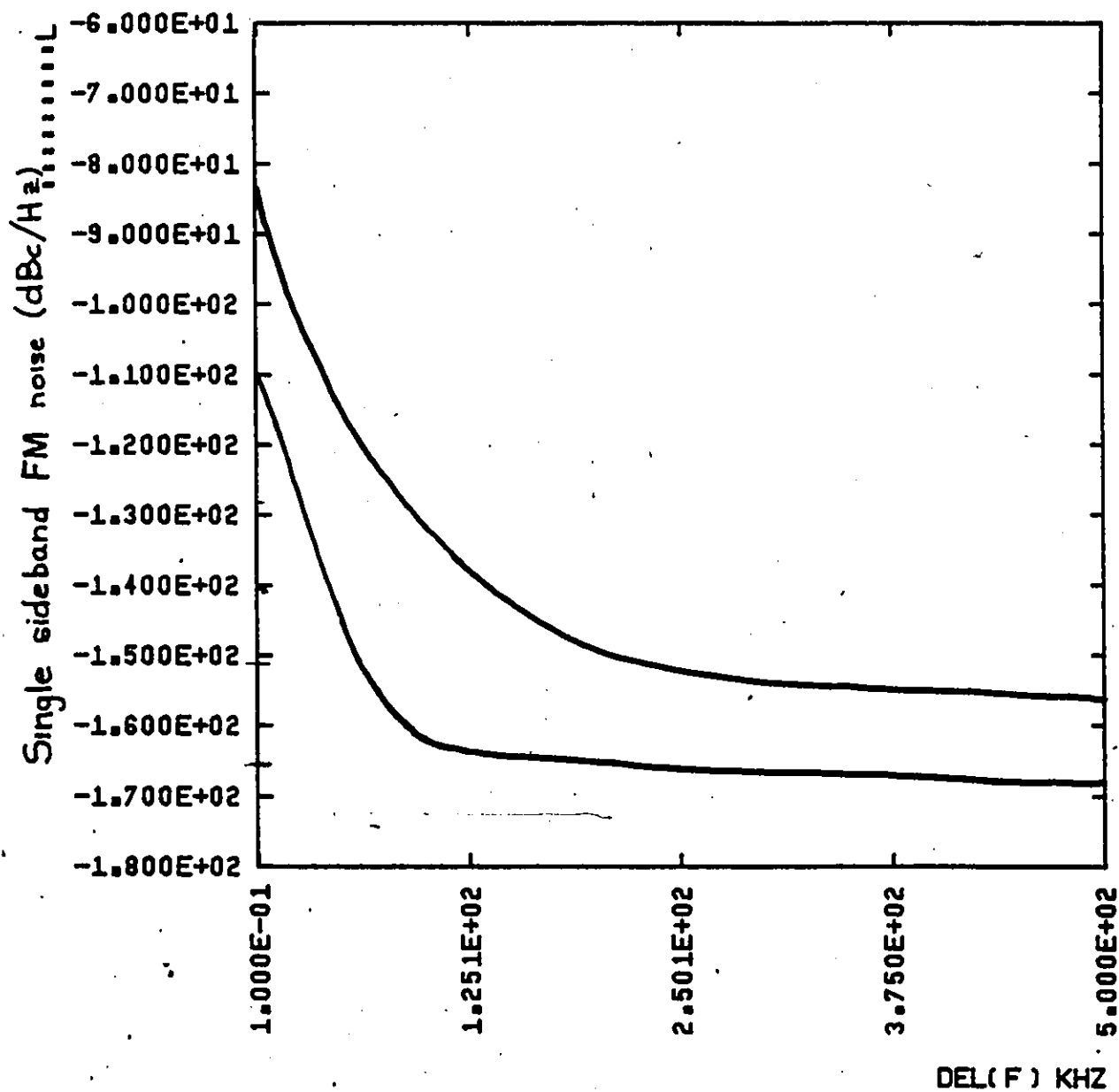


Figure 2.11 Measured noise performances of the delay line and the resonators. (Parker's report [26].)

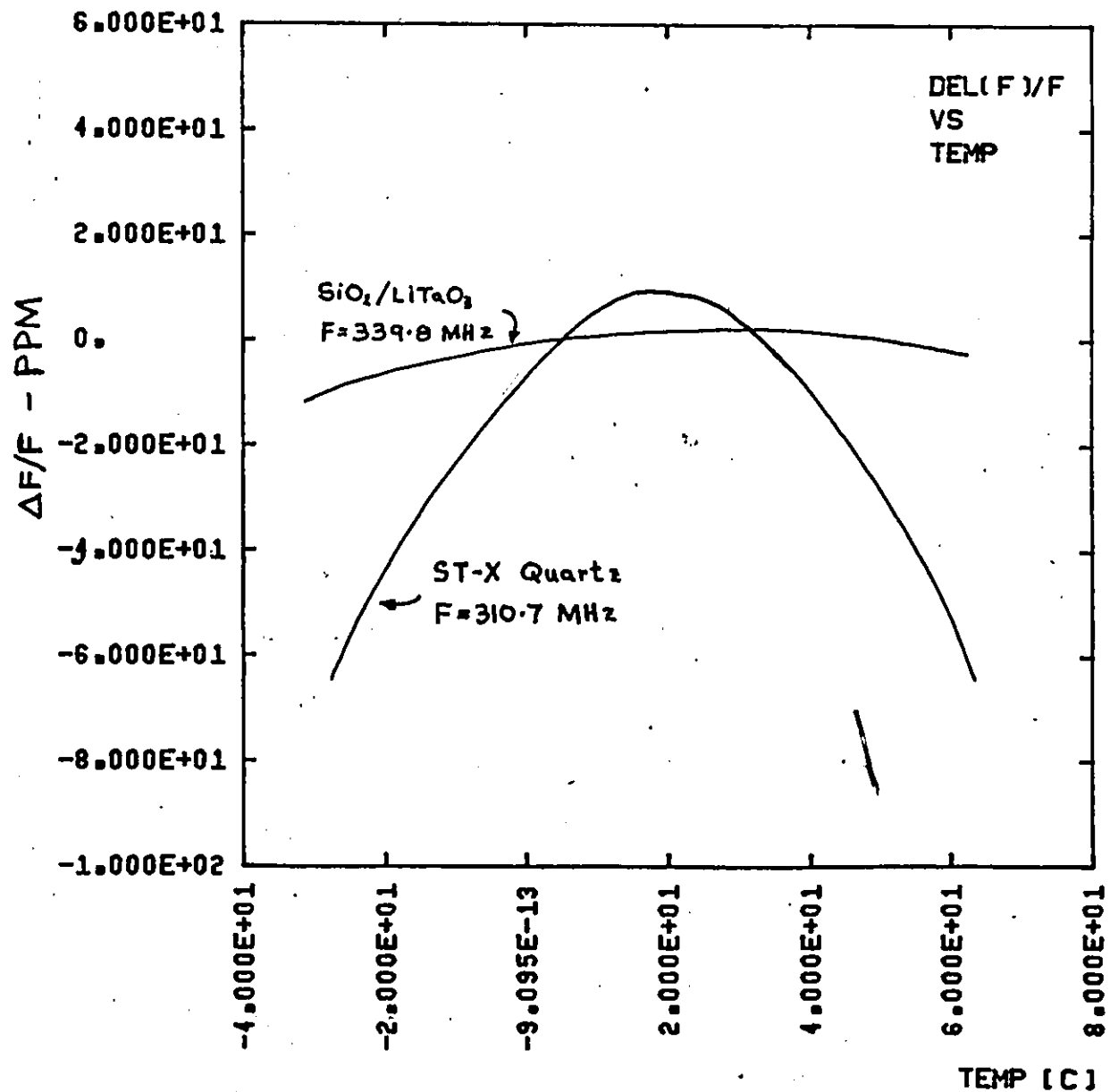


Figure 2.12 Temperature dependence of a  $\text{SiO}_2/\text{LiTaO}_3$  oscillator compared to an ST-X quartz oscillator (Parker and Schultz [26]).



the piezoelectric crystal and also on to another layer of  $\text{SiO}_2$ .

In the case where  $\text{SiO}_2$  is not used, the frequency will vary with temperature as follows [27]

$$f = f_0 (1 - 3 \times 10^{-8} (T - T_0))^2 \quad (2.5.11)$$

where  $f_0$  is the maximum frequency at  $T_0$ . Hence, increasing temperature will cause frequency to drift downward. If the temperature is held at  $T_0$  to within  $\pm 4^\circ\text{C}$  then the deviation will be less than 1 ppm [27].

Temperature variation also causes variation in the amplifier gains. This will cause phase variation in the feedback loop. Typically a temperature coefficient of about  $+ 0.5 \text{ ppm}/^\circ\text{C}$  could be attributed to the amplifier [26]. The ideal amplifier should have a high power, low-noise output, and a wide passband with the frequency of operation at the center of the bandpass. A comparison of SAW delay lines and resonators for medium term stability indicates that there is no significant difference between the two oscillator types in this respect [26].

### 2.5.3 Long-Term Stability

Long-term aging has been the problem area for the SAW oscillator, for both delay line and resonator types. The aging rates have been related to two areas; 1) cleaning and packaging and 2) acoustic power levels at which the

oscillator operates. Cleaning and packaging are very important, since frequency drifts vary with oxidation of the aluminum fingers, humidity and vibrations. Any organic components on the surface would degrade the aging performance of the device; hence the packaging should be accomplished as described in Appendix C.

The use of various metal alloy films on the substrate has demonstrated increases in stability [26]. A chromium and aluminum layer has proven to aid long term stability. Presently, use of a copper-aluminum alloy is being investigated by the author to improve stability in general.

Acoustic power levels above the threshold degrade the physical and electrical performance of the SAW oscillators. In particular, the effects of acoustic power on the adhesion of metallization to the substrate and the stresses within the substrate are currently under investigation at the Marconi Research Laboratories [21]. In general, resonators with input power of  $\leq 1\text{mW}$  have shown to give good aging rate at the Marconi Research Laboratories [21], and higher levels can be used with delay lines with various alloys deposited on the surface of the substrate.

## 2.6 Circuit Complexity and Fabrication

There are two major differences between the delay line and resonator oscillator which have impact on the complexity

of the oscillator. Both differences relate to the criteria for oscillation, as discussed above. The first is that the increased insertion loss of the delay line must be compensated by increasing the gain in the amplifier stage. Delay line-type oscillators are usually built on ST-X quartz crystal substrates and on lithium niobate ( $\text{LiNbO}_3$ ) substrates. The quartz is used when temperature stability is very important, since quartz has a zero temperature coefficient (1st order term), whereas  $\text{LiNbO}_3$  is used for short term stability because  $\text{LiNbO}_3$  delay lines have an insertion loss of the order of 20 dB or less; thus usually requiring only one amplifier package in the oscillator circuit. ST-X quartz, however, has typical insertion losses  $\geq 40$  dB requiring two or more miniature broadband amplifiers in cascade.

Secondly, the inability to specify the insertion phase of the delay line necessitates the use of a static phase shifter. This phase shifter, besides increasing board space, must be set to some value determined by a measurement of each delay line. This problem does not exist in the resonator, for which no phase shifter is required. The resonator does require the use of a shunt inductor to resonate the static capacitance of the transducer.

From a manufacturer's point of view, the difference in the cost to set up fabricating equipment and test equipment,

for either the resonator or the delay line is of no significance. However, there is significant differences that relate to fabrication techniques, sensitivity to variation in fabrication and also upper limits on frequencies that can be reached.

In delay lines, pattern defects pose a major problem in overall performance of the device. Though broken fingers or pinholes in the deposited aluminum pose no serious error in the short term, they do degrade the devices performance. SAW delay lines cannot function if there are shorts present between the finger pairs of the IDT. The center transducer on the resonator device is susceptible to the same defects as that of the delay line, but the transducer occupies only a small percentage of the total surface area of the resonator.

Control of metal film thickness to within  $100 \text{ \AA}$  was found to be necessary to insure that the measured frequency corresponded to the design value. As the thickness of metal increases the frequency shift is much greater than predicted by theory [29]. Experiments conducted in this thesis study, as illustrated in Table II, show about a 200 kHz shift in frequency for every  $300 \text{ \AA}$  of Al deposited. In the resonator the sensitivity to metal film thickness is somewhat lower than that of the delay line, but the control of the depths of the grooves and their widths is more important. Small

TABLE II

Variations in operating frequency due to variations of metal thickness.

| Metal Thickness ( $\text{\AA}$ ) | $f_o$ (Design) [MHz] | $f_o$ (Measured) [MHz] |
|----------------------------------|----------------------|------------------------|
| 500                              | 407.67               | 408.163                |
| 800                              | 407.67               | 408.375                |
| 1,200                            | 407.67               | 408.625                |
| 1,500                            | 407.67               | 408.908                |
| 1,800                            | 407.67               | 408.135                |

NOTE: There is a trade off as to the amount of Al deposited. If the film is too thin, it will oxidize very quickly. If it is too thick, mass loading becomes a major problem.

variations in  $(h/\lambda)$ , the depth to wavelength ratio, have significant impact on the performance of the resonator as reported by Williamson [16].

SAW delay line fabrications use chemical etching procedures to remove metal. In resonator fabrications, however, the grooves are etched into the crystal surface. Hence if an error results in the latter process (i.e. too deep) then the crystal is wasted, whereas the delay line can have the metal completely removed and, the crystal can be used again. Control of the chemical etching is crucial for the delay line since the metallization ratio will change as a function of the time of chemical etching. If the chemical etching is prolonged, undercutting will result and pinholes on the metal surface will appear.

The most common fabrication techniques for producing SAW devices are photolithography and electron beam lithography. Both methods have upper and lower frequency limits. Photolithography has a range of  $f = 0.5 - 300$  MHz when applied to SAW transducers where the upper attainable frequency is limited by linewidth resolution. The ordinary non-conformable contact mask is only capable of reproducing patterns with minimum linewidths of 4 microns. For some cases split electrodes are required to reduce reflections; hence the achievable frequency is further limited by linewidth resolution of the pattern.

Electron beam lithography does not use a contact mask. The obtainable line width is in the submicron region; hence, the attainable frequency range for SAW-transducer operation is  $f = 800 - 3200$  MHz. The disadvantage of this technique is that the field of view over which accurate resolution can be obtained, is limited. Both the delay line-type and resonator-type oscillators have these frequency restrictions since both structures contain IDT fingers.

One solution for overcoming these frequency limitations is to generate harmonics of the fundamental frequency. Until recently, harmonic generation has been limited to a 3-finger, 4-finger geometry (see thesis by P. Naraine [30], p. 29-35). However, research on harmonic generation by P. Narain, C.K. Campbell and Y. Ye [39] has successfully illustrated that higher order harmonics can be generated while suppressing all unwanted harmonics. IDT structures used to generate higher harmonic modes can be built using photolithographic techniques. The mask generated is referred to as the stepped-finger delay line [39]. In the next Chapter the stepped-finger delay line will be discussed in more detail and it will be shown that oscillators working at harmonics do perform as well as those operating at the fundamental.

## CHAPTER III

### DESIGN OF SAW DELAY LINES

#### 3.1 Substrate Considerations

The two most commonly used substrate materials for SAW devices are lithium niobate ( $\text{LiNbO}_3$ ) and ST-X quartz. Their general properties are illustrated in Figure 3.1 [32]. As seen from this figure,  $\text{LiNbO}_3$  materials exhibit a higher temperature coefficient and a higher surface wave velocity. The major difference between the two is in the coupling coefficient  $k^2$ , which is the measure of the efficiency by which electrical energy can be converted into mechanical energy on a piezo electric surface. The coupling coefficient can be expressed in terms of the material properties (dielectric constants,  $\epsilon_{PR}^T$ , and  $\Delta v_a/v_a$ , the fractional change in SAW velocity when a thin, massless conductor is deposited on the surface) [32].

$$k^2 = 2 \left( 1 + \frac{1}{\epsilon_{PR}^T} \right) \frac{\Delta v_a}{v_a} \left( 1 - \frac{\Delta v_a}{v_a} \right) \quad (3.1.1)$$

where [32]

$$\epsilon_{PR}^T = \frac{1}{\epsilon_0} (\epsilon_{11} \epsilon_{33} - \epsilon_{13}^2)^{1/2} \quad (3.1.2)$$



| Material         | Orientation           | $\frac{v_a}{v_m}$<br>m/s | $\frac{\Delta v_a}{v_m}$ | $k^2$<br>(measured) | Temperature<br>Coeff. of Delay<br>$\mu\text{m}/^\circ\text{C}$ | $C_{FF}$ in F/m<br>for $L_d = 0.5$ | Attenuation<br>at 1 GHz<br>dB/ $\mu\text{sec}$<br>in Air | $T$<br>CPR |
|------------------|-----------------------|--------------------------|--------------------------|---------------------|--|------------------------------------|--|------------|
| $\text{LiNbO}_3$ | Y,Z                   | 3488                     | 0.0241                   | 0.045               | 85   | $4.6438 \times 10^{-10}$           | 0.88   | 50.2       |
| $\text{LiNbO}_3$ | 41.5°X                | 4000                     | 0.028                    | 0.057               | 67   | $6.1857 \times 10^{-10}$           | 0.75   | 67.2       |
| Quartz           | Y,X                   | 3159                     | 0.0009                   | 0.0023              | -24  | $5.00664 \times 10^{-11}$          | 2.15   | 4.52       |
| Quartz           | ST,X<br>(Y+42 3/4° X) | 3153                     | 0.0006                   | 0.0016              | 0  | $5.03385 \times 10^{-11}$          | 2.62   | 4.55       |

Fig. 3.1 The most commonly used piezoelectric substrates and their general properties.

The primary consideration in this thesis was not to obtain good temperature stability, which would have required the use of quartz crystal. In particular, the ST-quartz\* crystal is the more suitable choice for temperature stability since it has a first-order temperature coefficient of 0 ppm/°C and a second order coefficient of  $31.5 \times 10^{-9}$  ppm/°C.

The purpose of this thesis is to experimentally illustrate that oscillators can be built using delay lines operating at one of the harmonics of IDT frequency operation.  $\text{LiNbO}_3$  was the substrate chosen because it simplified the circuit complexity since only a single amplifier package was used.

### 3.2 Design of the Stepped-finger IDT Structure

#### 3.2.1 Introduction

To date, there have been reports (M. Lewis [27]) of oscillators operating at a 310 MHz fundamental frequency. However, the photolithographic facilities at McMaster University limit the fundamental frequency at which SAW delay lines can operate (i.e.  $\approx$  185 MHz upper limit). If

---

\* The abbreviation "ST" stands for the cutting angle of the quartz crystal. The angle at which the quartz is cut, effects the temperature coefficient on the substrate [32].

the oscillator can operate at the harmonic frequencies of the delay line then it is possible to build delay lines with a fundamental of 150 MHz operating at any higher harmonic, say up to the 9th maximum, resulting in an operating frequency of 1.35 GHz. One of the more difficult problems arising from the use of transducers operating at a higher harmonic mode, is that other harmonics will interfere with the desired frequency. In Figures 3.2, 3.3, 3.4, plots of the spatial harmonics as a function of  $m$  (the metallization ratio) are illustrated, for the 2-finger, 3-finger and 4-finger structures [30]. As shown in the plots, depending on the value of the metallization ratio, more than one harmonic can be generated at the same time. This was experimentally verified by S.J. Kerbel [33]. With the stepped-finger design, the desired harmonic mode is isolated from the remaining unwanted modes. The above discussion on mode selection, deals only with the fundamental modes. Here a second mode selection must be considered to operate the oscillator at a higher frequency.

### 3.2.2 Theory of the Stepped Finger Delay Line

Waves launched from a uniform transducer, such as the 2-finger transducer, shown in Figure 3.5(a), have the same phase angle along its length. The stepped-finger transducer shown in Figure 3.5 (b) has its fingers divided into

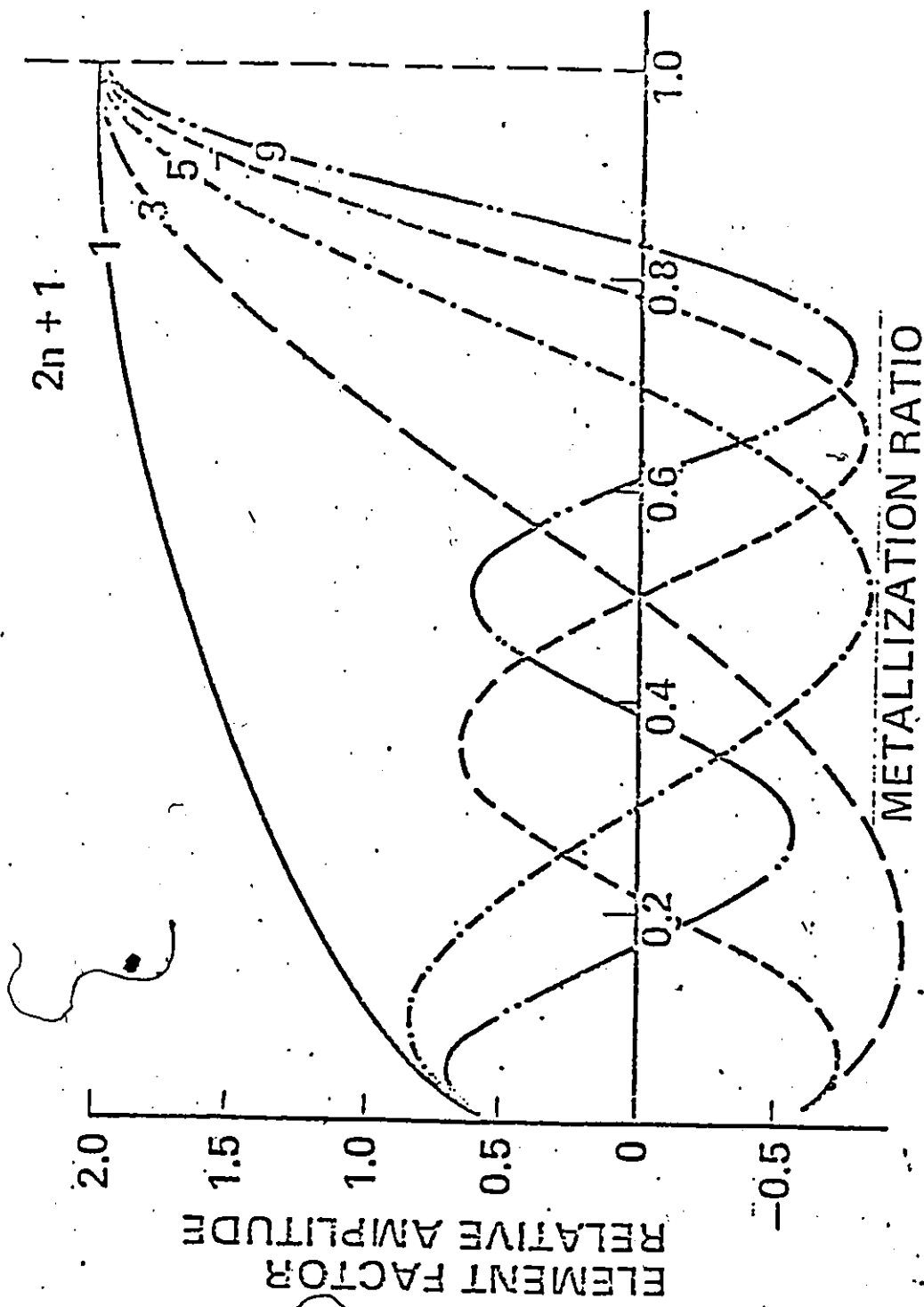


Fig. 3.2 Amplitude of the five lowest spatial harmonics as a function of  $n$  for the 2-finger geometry transducer.

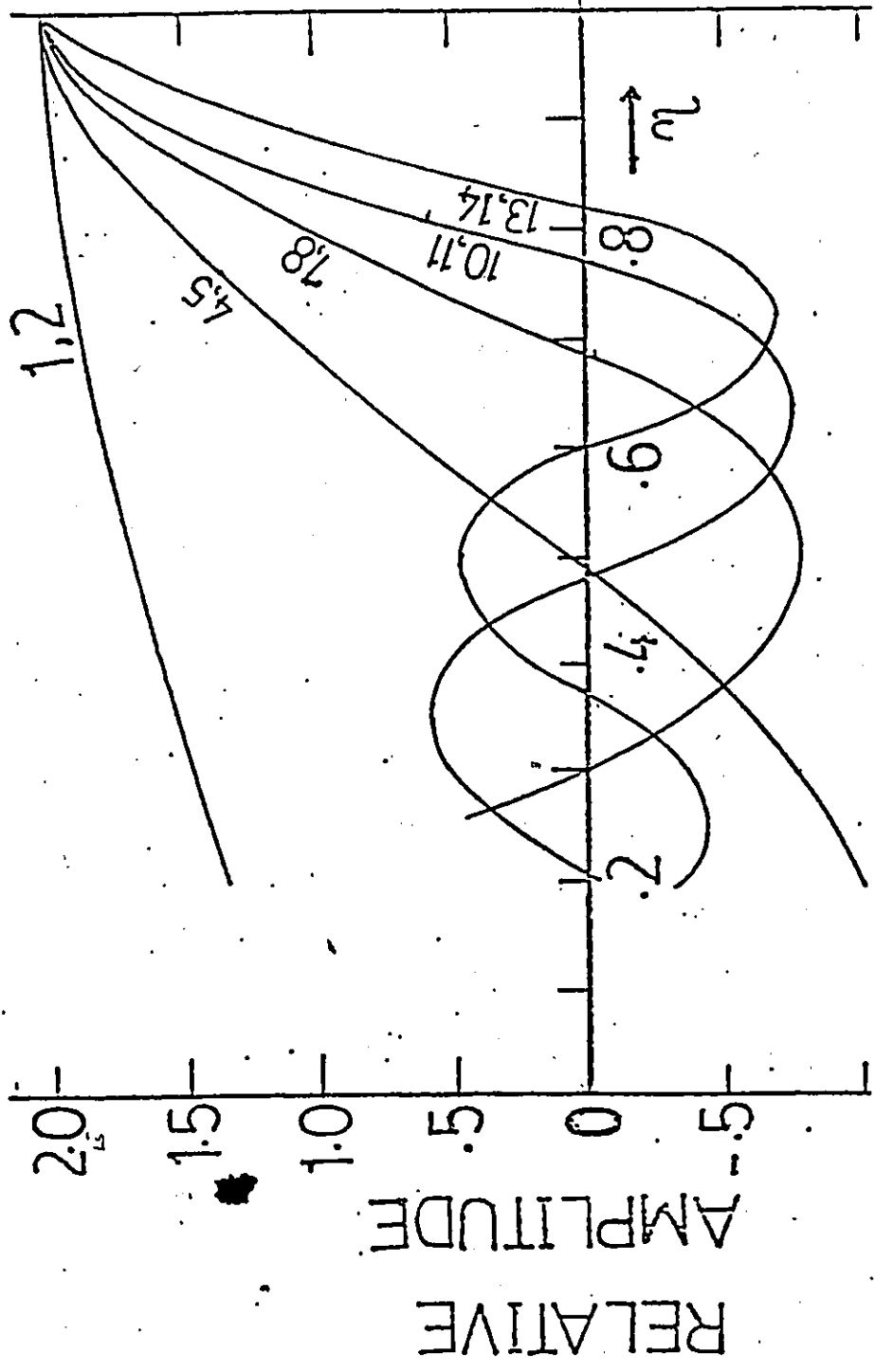


Fig. 3.3 Amplitude of 15 lowest spatial harmonics of the 3-finger geometry transducer.

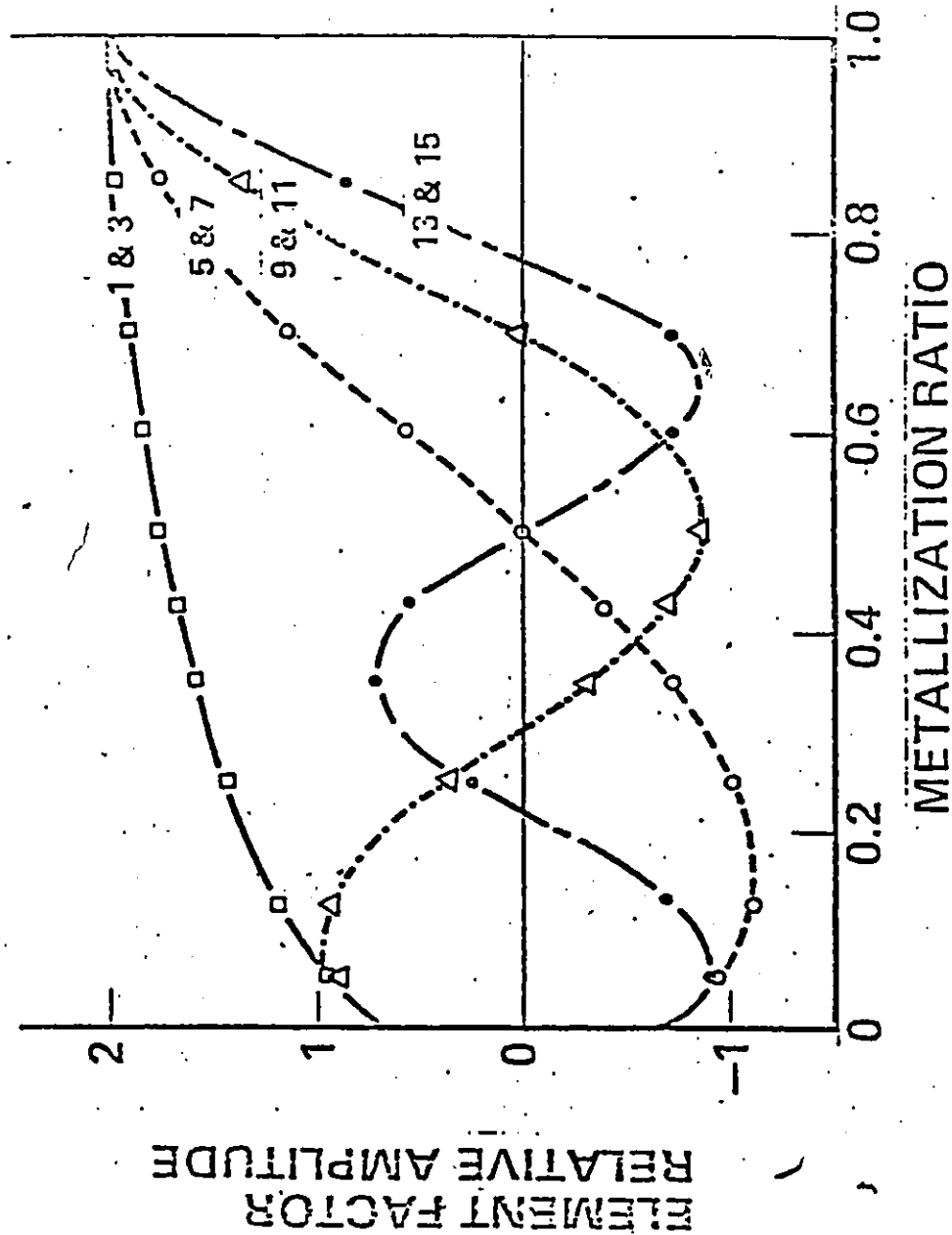


Fig. 3.4 Amplitude of 15 lowest spatial harmonics of the 4-finger geometry transducer.

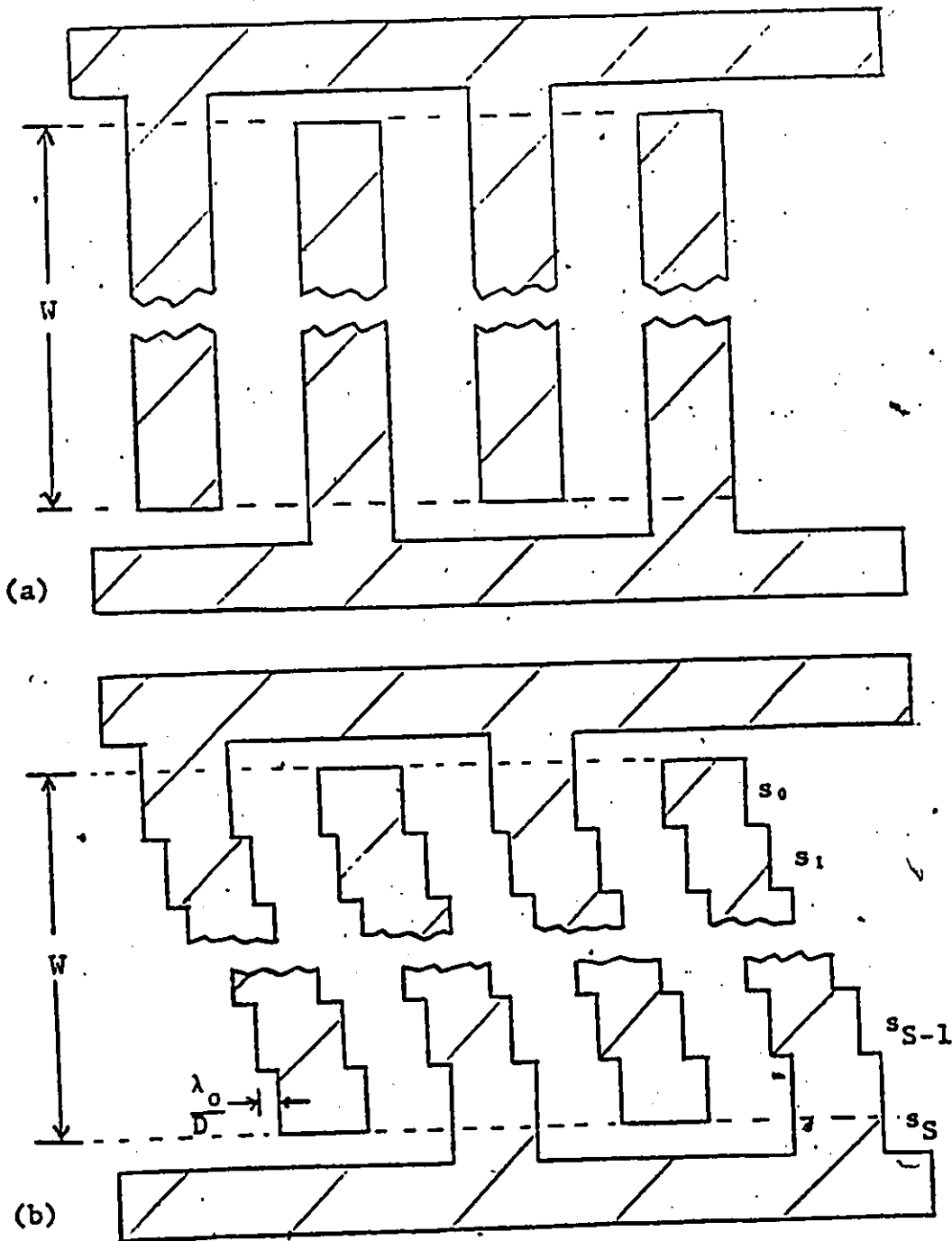


Fig. 3.5 (a) The classical finger structure with each section along its length at the same phase angle.

(b) The stepped-finger structure with each segment along its length displaced from each other by  $\frac{\lambda_0}{D}$ .

segments, each equally displaced from one another. The amount of displacement is a fraction of the fundamental wavelength,  $\lambda_0/h$ , as shown in Figure 3.5(b). The phase difference between the adjacent segments on one finger will be  $2\pi M/h$  where  $M$  is the harmonic mode,  $h$  is the displacement constant ( $h = M_d$ , where  $M_d$  is the desired harmonic mode).

At a summing point  $P$  the resultant wave  $R(f_M)$  at any harmonic mode  $M$ , will be the phasor sum of the waves generated by each segment

$$R(f_M) = \sum_{s=1}^{M_d} A(f_M) \underline{s(2\pi M/d)} \quad (3.2.1)$$

where

$s$  is the total number of segments on each finger,  
 $A(f_M)$  is the amplitude of the wave generated by each segment at frequency  $f_M$ .

At the receiving transducer the desired resultant waves must add up in phase. Hence if each segment is displaced by  $\lambda_0/M_d$  and each finger is divided equally into  $M_d$  segments (i.e.  $S = M_d$ ), then (3.2.1) reduces to

$$\begin{aligned} R(f_{M_d}) &= \sum_{S=1}^{M_d} A(f_M) \underline{s(2\pi M_d/M_d)} \\ R(f_{M_d}) &= \sum_{S=1}^{M_d} A(f_M) \underline{s(2\pi)} \\ R(f_{M_d}) &= M_d A(f_M) \end{aligned} \quad (3.2.2)$$

The resultant wave at the undesired harmonic modes results



in

$$R(f_M) = \sum_{s=1}^{M_d} A(f_M) \frac{1}{s(2\pi M/M_d)}$$

$$R(f_M) = 0 \quad (3.2.3)$$

Equations (3.2.2) and (3.2.3) indicate that with displacement  $d = \lambda_0/M_d$  and  $S = M_d$  the desired harmonic mode  $M_d$  will add constructively and undesired harmonics will exhibit internal suppression.

To calculate the transfer function of the stepped-finger transducer, each stepped-finger is treated as an end-fire antenna array consisting of  $M_d$  elements with each element displaced  $\lambda_0/M_d$  from its neighbour; the transfer function of this array being the one-sided Z-transform, which reduces to the form given in (3.2.5) (see P. Naraine [30], pp. 51-52).

$$H(z) = \sum_{n=0}^{M_d-1} a_n z^{-n} \quad (3.2.4)$$

where

$$z = e^{-j\theta}$$

and

$$\theta = 2 \frac{f - f_{M_d}}{f_{M_d}}$$

Equation (3.2.4) reduces to the form

$$H(f) = \frac{\sin[\pi(f-f_{M_d})]/f_o}{\sin[\pi(f-f_{M_d})]/f_M} \quad (3.2.5)$$

The overall transfer function of the stepped-finger transducer  $|H(f)|$  is given by the product of the transfer function for a classical uniform transducer,  $|H_1(f)|$  and the transfer function for the stepped-finger transducer,  $|H_2(f)|$

$$|H(f)| = |H_1(f)| |H_2(f)| \quad (3.2.6)$$

where

$$|H_1(f)| = \left| A_M \right| \frac{\sin[2\pi N(f-f_M)]/f_M}{[2\pi N(f-f_M)]/f_M}$$

and

$$|H_2(f)| = \frac{\sin[\pi(f-f_{M_d})]/f_o}{\sin[\pi(f-f_{M_d})]/f_{M_d}}$$

### 3.2.3 Equations and Calculations for Stepped-Finger Delay Lines

The SAW delay line was chosen to operate at a harmonic frequency,  $f_M = 407.6 \text{ MHz}$ . The 5th harmonic was chosen to be the desired harmonic mode (i.e.,  $M_d = 5$ ). The metallization ratio was chosen to be 50% (i.e.,  $n = 0.5$ ) since only the fundamental, 5<sup>th</sup> and the 9<sup>th</sup> harmonics would be present (see Figure 3.2). The input transducer was designed to have an input impedance of 50  $\Omega$ .

The delay line was designed at the fundamental

frequency  $f_o$ ,

$$f_o = \frac{f_{M_d}}{M_d} \quad (3.2.7)$$

$$f_o = \frac{407.67}{5} \text{ [MHz]}$$

$$f_o = 81.53 \text{ [MHz]}$$

The corresponding wavelength is

$$\lambda_o = \frac{v_s}{f_o} \quad (3.2.8)$$

where  $v_s$  is the SAW velocity for  $\text{LiNbO}_3$  (see Figure 3.1),

$$\lambda_o = \frac{3488}{81.53 \times 10^6} \text{ [m]}$$

$$\lambda_o = 42.94 \times 10^{-6} \text{ [m]}$$

The design equations for the stepped-finger transducer are similar to that of the 2-finger transducer. With reference to Figure 2.4, the sum of the finger width,  $X$  and the gap between fingers,  $Y$  is,

$$X + Y = \frac{\lambda_o}{2} \quad (3.2.9)$$

The metallization ratio ( $n$ ) is defined as

$$\frac{X}{X + Y} = n \quad (3.2.10)$$

Hence for  $n = 0.5$

$$\frac{X}{X+Y} = 0.5$$

From (3.2.8) and (3.2.9)

$$X = \frac{\lambda_0}{4}$$

$$X = 10.736 \times 10^{-6} \text{ [m]}$$

Similarly,

$$Y = Y$$

$$Y = 10.736 \times 10^{-6} \text{ [m]}$$

Since the desired harmonic is the fifth, each finger must be divided into 5 equal segments. The displacement of each segment from its neighbour, is

$$d = \frac{\lambda_0}{5} \quad (3.2.11)$$

$$d = \frac{42.94 \times 10^{-6}}{5} \text{ [m]}$$

$$d = 8.588 \times 10^{-6} \text{ [m]}$$

The width of each segment is determined by dividing the aperture by the number of segments. The aperture width directly relates to the capacitive susceptance of the transducer. For minimum untuned insertion loss, the input transducers' capacitive susceptance must be made equal to the admittance of the source. For a 50  $\Omega$  source (i.e.,  $Z_{11} = 50 \Omega$ ),

$$Z_{11} = \frac{1}{|2\pi f_5 C_{T1}|} \quad (3.2.12)$$

$$C_{T1} = \frac{1}{2\pi f_5 Z_{11}} \text{ [F]}$$

$$C_{T1} = \frac{1}{2\pi (407.67 \times 10^6) (50)}$$

$$C_{T1} = 7.808 \text{ [pF]}$$

where  $C_{T1}$  is the total capacitance for the input transducer.

Choosing the total number of finger pairs at the input transducer to be 150 (i.e.  $N_1 = 150$ ), the aperture width is calculated from (3.2.13),

$$W = \frac{C_{T1}}{C_{FF} N_1} \quad (3.2.13)$$

where  $C_{FF}$  is the static capacitance given by (3.2.14)

$$C_{FF} = 2(\epsilon_{PR}^T + 1) [6.5 n^2 + 1.08 n + 2.37] \left[ \frac{\text{pF}}{\text{m}} \right] \quad (3.2.14)$$

where  $\epsilon_{PR}^T$  is defined by (3.1.2). For  $\text{LiNbO}_3$   $\epsilon_{PR}^T$  has a value  $\epsilon_{PR}^T = 50.2$  (see Figure 3.1).

Hence for  $n = 0.5$  and using  $\text{LiNbO}_3$ ,

$$C_{FF} = 2(50.2 + 1) [6.5(0.5)^2 + 1.08(0.5) + 2.37] \left[ \frac{\text{pF}}{\text{m}} \right]$$

$$C_{FF} = 4.64 \times 10^{-10} \left[ \frac{\text{F}}{\text{m}} \right]$$

Hence

$$W = \frac{7.808 \text{ pF}}{(4.64 \times 10^{-10}) (150)}$$

$$W = 112.18 \times 10^{-6} \text{ [m]}$$

The width of each segment is

$$W_s = \frac{W}{M_d} \quad (3.2.15)$$

$$W_s = 22.436 \times 10^{-6} \text{ [m]}$$

The segment width,  $W_s$  calculated above is a very impractical size to produce the artwork and mask of the delay line, hence, the value of  $W_s$  was increased to  $100 \times 10^{-6}$  [m].

The output transducer was designed using the conventional 2-finger geometry. The physical dimensions were calculated from the fundamental frequency  $f_0 = 81.53$  MHz. Hence all the cutting parameters were identical to that of the stepped-finger design, (i.e.  $X = Y = 10.74 \times 10^{-6}$  [m]  $W = 100 \times 10^{-6}$  [m]). Though the aperture of the output transducer was equal to that of the input transducer, the bandwidth was designed slightly larger. This was accomplished by using 50 finger pairs at the output transducer (i.e.  $N_2 = 50$ ).

The null bandwidth can be approximated by (see Figure 3.5),

$$\%BW = \frac{f_1 - f_2}{f_{M_d}} \times 100 \quad (3.2.16)$$

where  $f_1, f_2$  are the null bandwidth points which occur at

$$f_1 = f_{M_d} - \frac{f_{M_d}}{N} \quad (3.2.17)$$

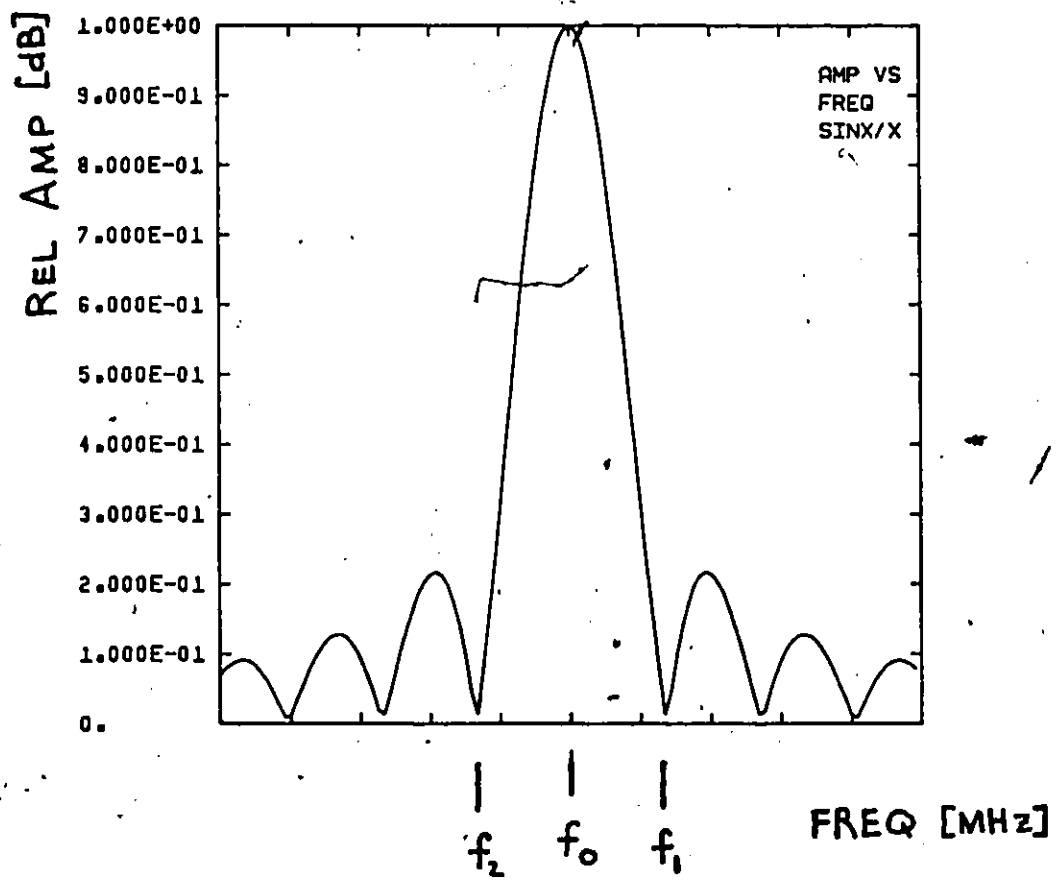


Figure 3.6 Calculation of Null Percentage Bandwidth.

$$f_2 = f_{M_d} - \frac{f_{M_d}}{N} \quad (3.2.18)$$

therefore

$$\%BW = \frac{(f_{M_d} + \frac{f_{M_d}}{N}) - (f_{M_d} - \frac{f_{M_d}}{N})}{f_{M_d}} \quad (3.2.19)$$

$$\%BW = \frac{2}{N} \times 100$$

Hence for the input transducers,  $N_1 = 150$

$$\%BW = \frac{2}{150} \times 100 = 1.3\%$$

At the output transducer,  $N_2 = 50$

$$\%B = \frac{2}{50} \times 100 = 4.0\%$$

Also, the capacitance of the output transducer is

$$C_{T_2} = W C_{FF} N_2 \text{ [pF]} \quad (3.2.20)$$

$$C_{T_2} = (112 \times 10^{-6}) (4.64 \times 10^{-10}) (50)$$

$$C_{T_2} = 2.60 \text{ [pF]}$$

The input transducer has a time delay which can be approximated by [15]



$$\tau_p = \left( \frac{N_1 + 60}{2 f_{M_d}} \right) + 0.5 \text{ [}\mu\text{sec]} \quad (3.2.21)$$

Hence, with  $N_1 = 150$

$$\tau = 0.19 \mu\text{sec}$$

Recall (2.4.9) for the calculation of the Q-factor.

$$Q = \pi N'$$

where

$$N' = \tau_d f_{M_d}$$

$$N' = (0.19)(407.67)\lambda$$

$$N' = 391.3 \lambda$$

therefore

$$Q = (\pi)(391.3)$$

$$Q = 1229$$

As discussed in Section 2.3, mode selection was accomplished by designing the delay line to have an effective length equal to the number of wavelengths in the input transducer, (i.e.  $l_d = N_1 \lambda$ ). Figure 3.7 is a detailed sketch of the stepped-finger delay line dimensions to be used in the SAW oscillator.

### 3.3 Fabrication of the SAW Delay Line Oscillator

#### 3.3.1 Construction of the Delay Line Circuit

The delay line circuit dimensions, as specified in the above section 3.2.3, were converted to inches and then

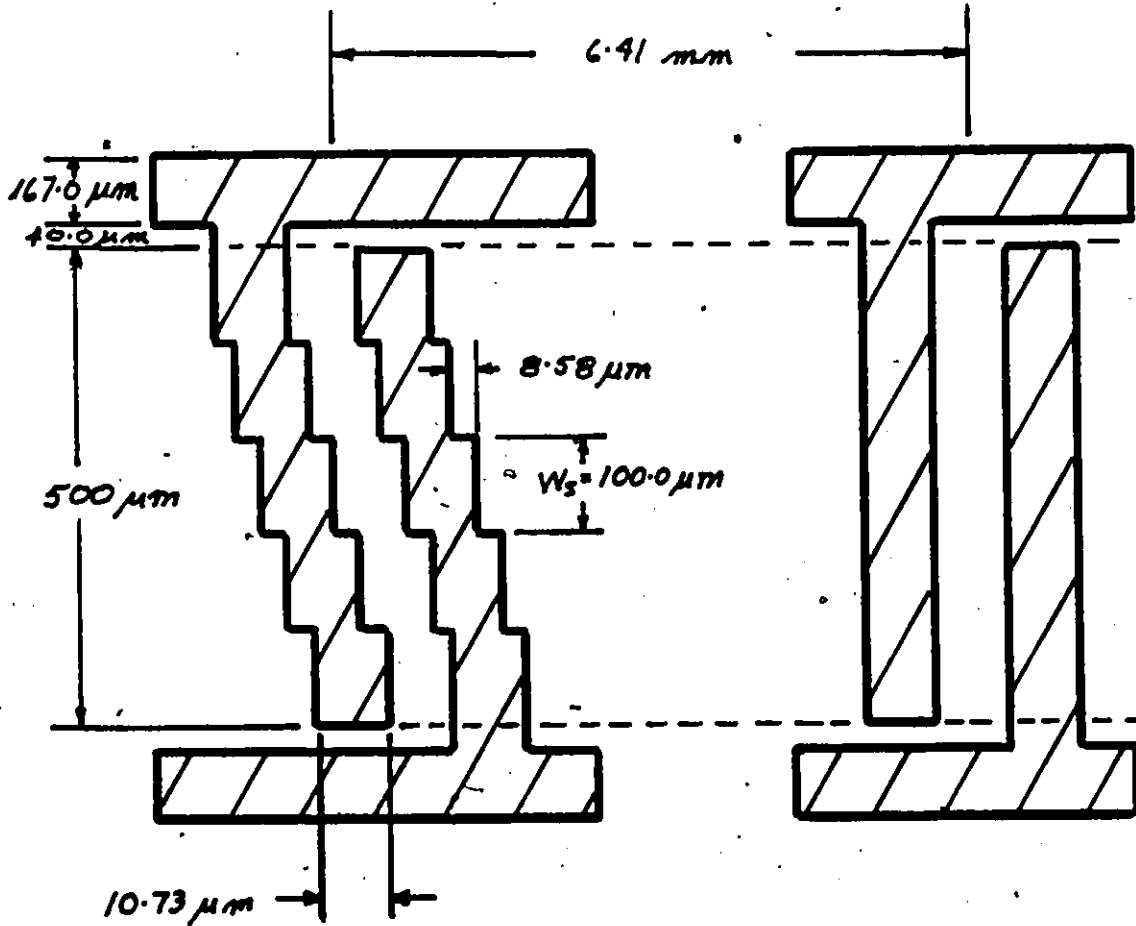


Figure 3.7 Detailed schematic of the stepped-finger delay.

scaled upward by a factor of 190. These dimensions were used to cut an enlarged positive pattern of the delay line on red rubylith (Ulano #07261), using a Haag Streit AG-1200 x 1200 mm cutting table, as illustrated in the photograph of Figure 3.8.

The procedure followed for preparing the circuit and transferring it to the substrate is that outlined in P. Naraine's thesis, p. 68-77 [30].

### 3.3.2 Construction of SAW Oscillator Circuit

The insertion loss of the delay line was less than 20 dB (see Chapter IV for further details). Hence, only one MIC amplifier with 20 dB gain was required. Specifications of the MIC amplifier are tabulated in Table III.

The substrate was glued to a Avantek TB-4 series circuit board using Apiezon sealing wax. Apiezon vacuum grease was placed at the edges of the substrate to prevent reflections of the acoustic waves from the edges. The MIC amplifier was soldered into the circuit board, and the entire circuit board, with mounted substrate and amplifier was inserted into a Avantek TC-4 Series Case. The bus bar of the input transducer was connected to the OSM type connectors. The output transducer was connected to the input of the MIC amplifier. All the bus bars which had to be grounded, were done so by connection to the case. All

Figure 3.8 Photograph of the cut delay line.



TABLE III

Amplifier Specifications

|   |                                      |
|---|--------------------------------------|
| TYPE                                      | AVANTEK UTO-512                      |
| Frequency Range                           | 5-500 MHz                            |
| Gain                                      | 20 dB                                |
| Flatness                                  | ± 1 dB                               |
| Noise Figure                              | 4.5 dB                               |
| VSWR (50L)                                | 2.0 max                              |
| Power output for 1 dB Gain<br>Compression | + 7 dB min                           |
| Intercept point for IM products           | + 20 dB m                            |
| Input Power                               | + 15 V @ 23 mA<br>(± 190 regulation) |
| Input/Output impedance                    | 50 L                                 |

Directional Coupler Specification

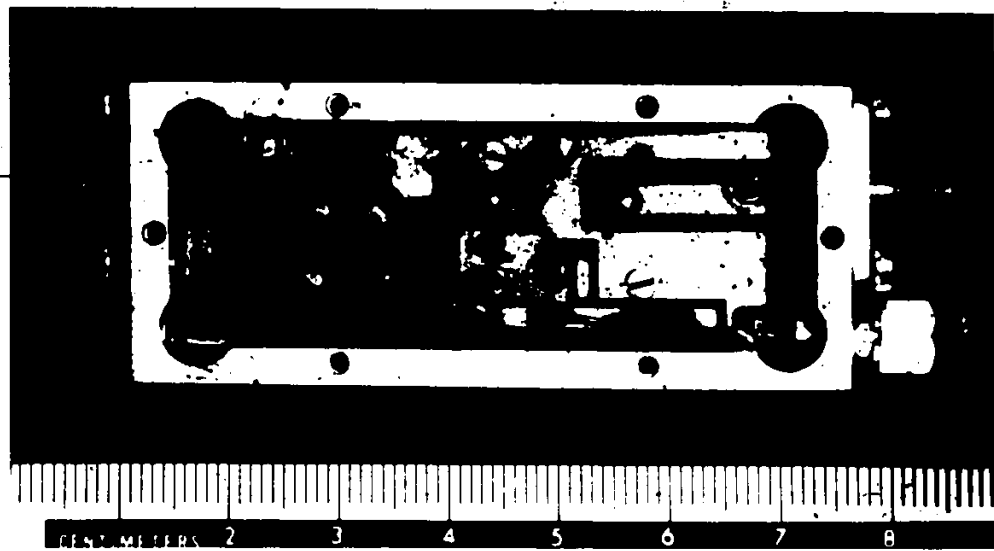
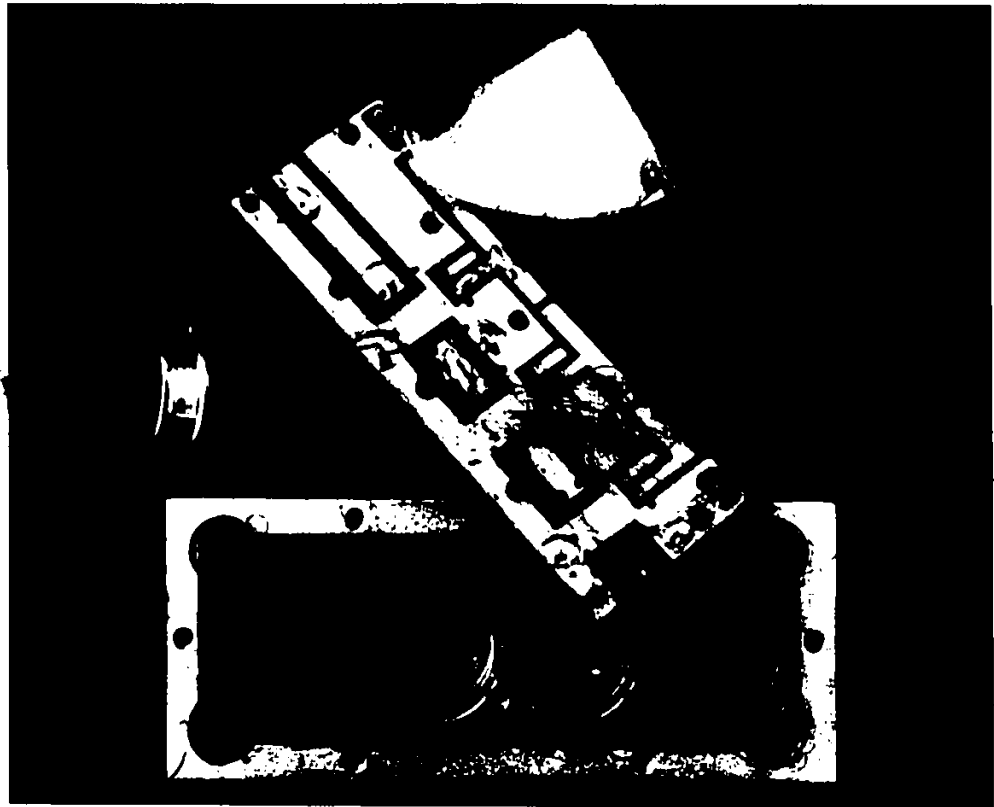
|                       |            |
|-----------------------|------------|
| TYPE CRM-10-500       | MERRIMAC   |
| Frequency Range       | 50-500 MHz |
| Coupling              | 10± 0.5 dB |
| Directivity           | 25 dB      |
| VSWR (50 ohms)        |            |
| Main Arm              | 1.3        |
| Coupled Arm           | 1.3        |
| Insertion loss        | 0.6 dB     |
| Input power (Maximum) | 5 watts    |

connections were made using 0.001" diameter, 99.99% gold wire and GC Silver Conductive Paint. Pictures of the delay line and case used are shown in Figure 3.9. A schematic of the designed 407.67 MHz SAW oscillator is shown in Figure 3.10. The feedback loop was externally completed using a 3 dB Merrimac directional Coupler (see Table III). Figure 3.11 shows a photograph of the final product.

Figure 3.9(a) Photograph of mounted delay line.

(b) Photograph of assembly of delay line and amplifier case.





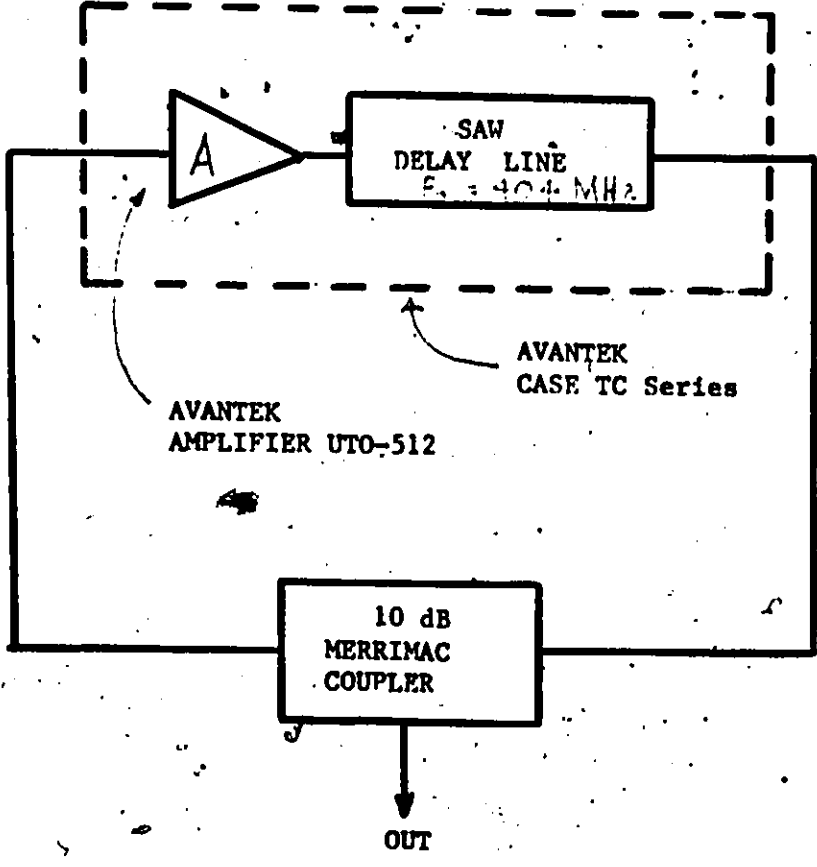


Figure 3.10 Schematic drawing of the SAW oscillator.

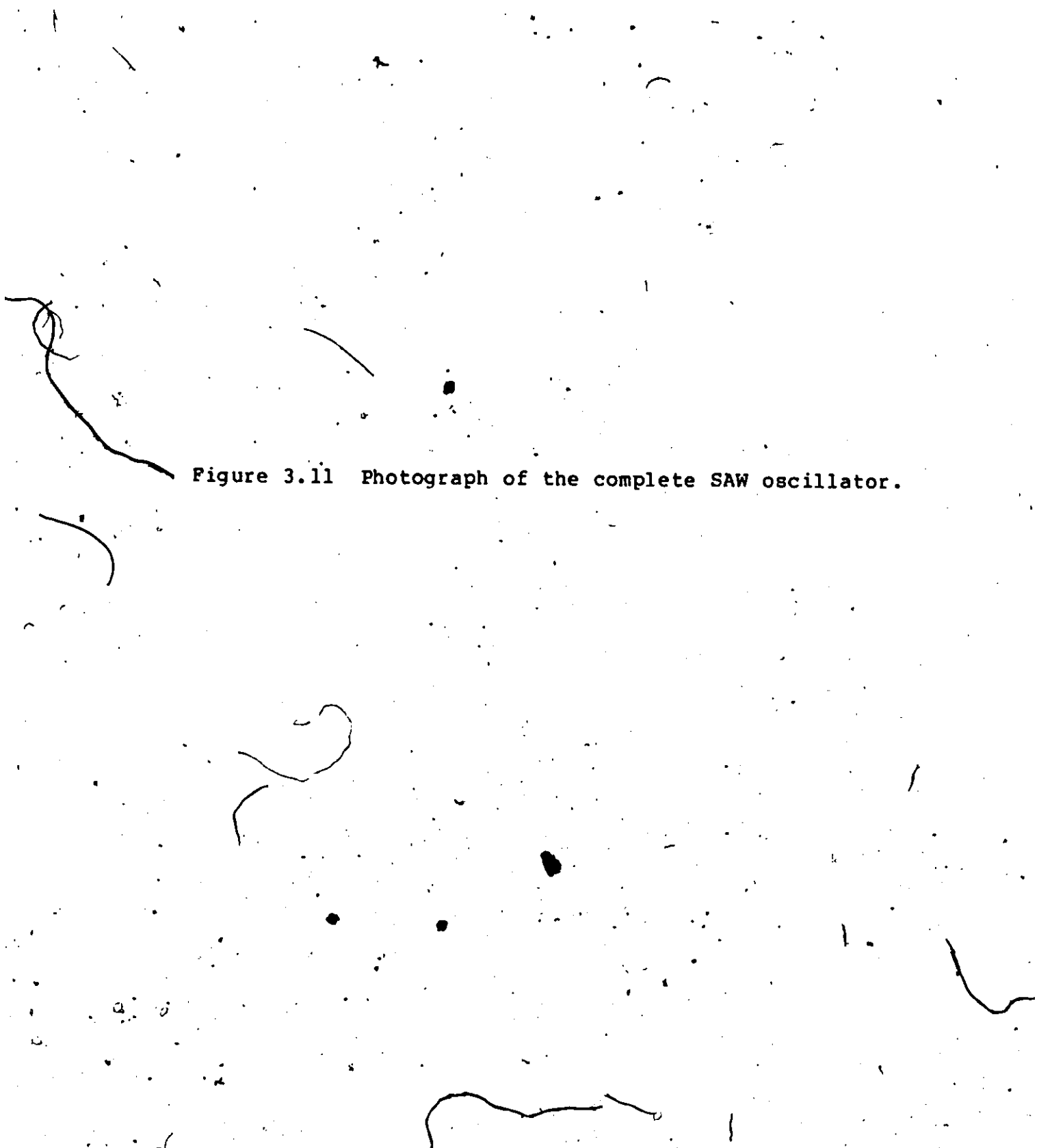
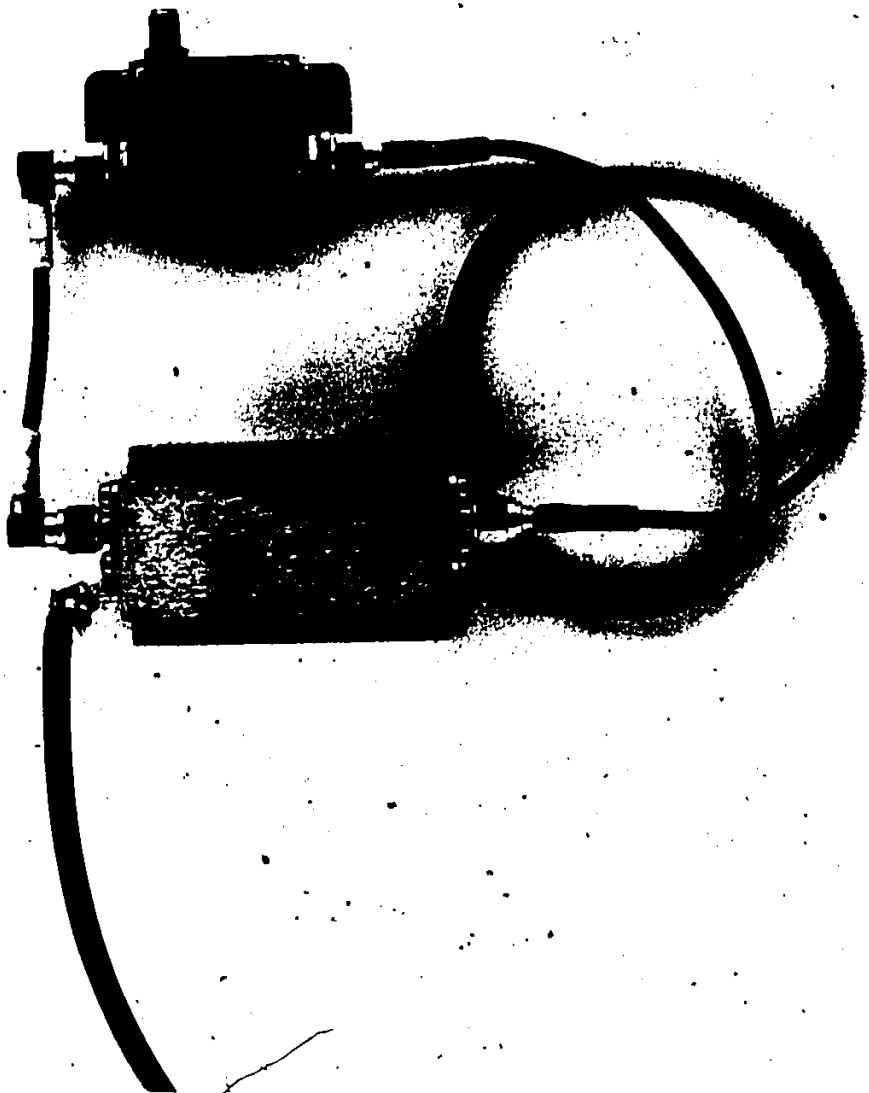


Figure 3.11 Photograph of the complete SAW oscillator.

F FISHER SCIENTIFIC



## CHAPTER IV

### RESULTS

#### 4.1 Delay Line Results

The amplitude response of the delay line and amplifier package shown in Figure 3.9(b) was measured using a Hewlett Packard 8505A Network Analysis with the Hewlett Packard 8501A Normalizer along with the 8502A Transmission/Reflection Test set (also from Hewlett Packard). Figure 4.1 shows the test set up for the delay line and the open loop oscillator. From this assembly the phase, group delay and the input/output impedance values were also measured. All connections were made with 50  $\Omega$  coaxial cable.

The input and output capacitance of the delay line was measured using a General Radio Capacitance Bridge 1615-A.

The frequency response of the first delay line fabricated and tested as shown in Figure 4.2(a). The frequency was swept from  $f_{\text{START}} = 25$  MHz to  $f_{\text{STOP}} = 425$  MHz. The fundamental frequency peaks at approximately -25 dB. The fifth harmonic frequency is not noticeable. The frequency response suffers severely from bulk wave interference, which is illustrated in the expanded view in Figure 4.2(b). Typical procedures were used to suppress bulk wave interference (i.e. the bottom surface of the

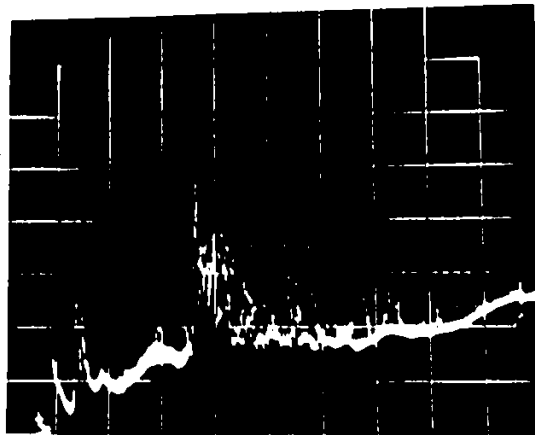
Figure 4.1 Photograph of the Hewlett Packard Network Analyser 8505A set up for testing of the delay lines.

708



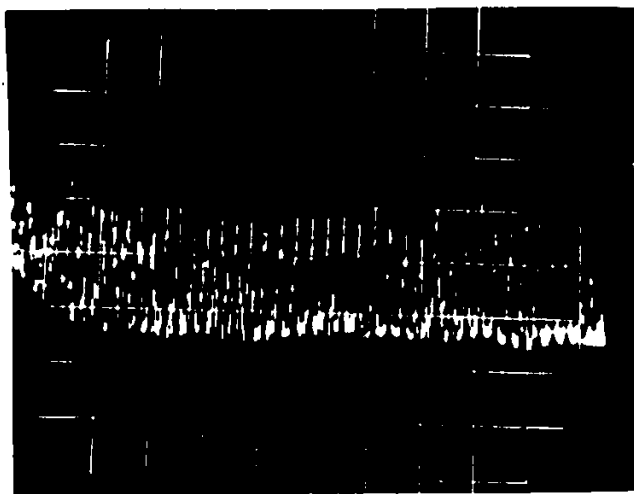
Handwritten scribbles and marks at the bottom of the page.

-10 dB —  
(ref.)



(a)

-10 dB —  
(ref.)



(b)

Figure 4.2(a) Frequency response of mismatched delay line.

(b) Bulk wave interference (expanded view).



substrate was rough and epoxy wax was used on the bottom surface to absorb the bulk waves) evidently other factors contributing to bulk wave generation were overlooked.

Reduction of bulk waves is outside the scope of this thesis, further details are given in reference [37].

By examining the design parameters it was found that the aperture  $W$ , of the delay line was too large, i.e.  $W = 40 \lambda$ . This value was chosen for ease of fabrication of the mask and circuit. By maintaining a large aperture, one reduces diffraction of the wave on the surface. From experiments conducted by the author it became apparent that the aperture was a crucial design parameter of the stepped-finger delay line. When designing the delay line above  $f_M = 200$  MHz the design dimensions  $W$ ,  $W_s$  and  $d$  must be as close as possible to the calculated values. Three reasons are postulated by the author as to why this constraint must exist.

First, there will be a mismatch at the input and output transducers. This would cause increase in insertion loss of the overall response. Secondly, since the output is designed with the same aperture and with more than 50 finger pairs, it is susceptible to coupling with the bulk waves within the substrate, hence resulting in a comb of peaks as shown in Figure 4.2(b). Thirdly, the width of each segment  $W_s$  was also very large, i.e.  $W = 40 \lambda$ ,  $M_d = 5$ , hence  $W_s = 8\lambda$ .

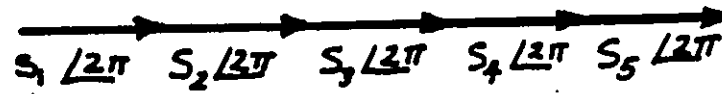
Each segment behaves as if it was a 2-finger transducer on its own. The neighboring segments introduce a phase error to the adjacent segments. Hence, the internal harmonic suppression is no longer operating.

The operating of the stepped-finger delay line essentially depends on the summation of the phase of the harmonic frequencies at the output transducer. If the input impedance is not matched to  $Z_{11}$ , i.e.  $Z_{11} = 50 \Omega$  and hence the capacitance  $C_{T1}$  is too large (both due to a large aperture), a phase error is introduced at each segment. Thus the calculation of the resultant wave  $R(f)$  from (3.2.1) becomes

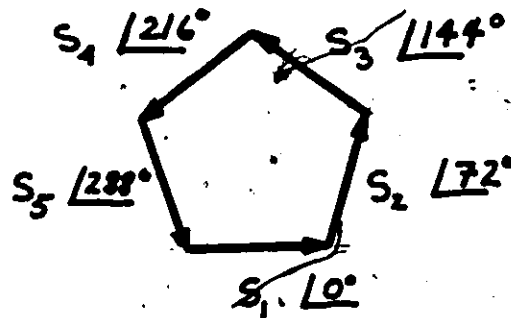
$$R(f) = \sum_{s=1}^{M_d} A(f_m) / \sqrt{s(2\pi M/M_d) + \phi_M} \quad (4.4.1)$$

Figure 4.3 illustrates the summation of the phase of an ideal stepped-finger delay line, at the desired harmonic frequency and at the fundamental frequency (same applies to the unwanted harmonics). Figure 4.4 shows the effect that phase error, from each segment, can have on the internal harmonic suppression mechanism of the delay line.

Figure 4.5(a) illustrates the frequency response of a stepped-finger delay line built identical to that the first delay line but with the aperture reduced to  $W = 15 \lambda$ , (hence  $W_B = 3\lambda$ ). The result is that the properly matched delay line had the fifth harmonic frequency peaking at -21 dB.



$$R(f) = 5A(f)$$

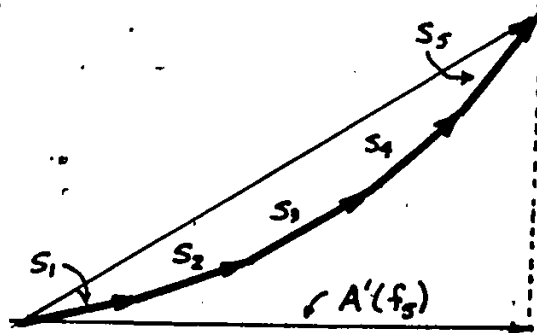


$$R(f) = 0$$

(b)

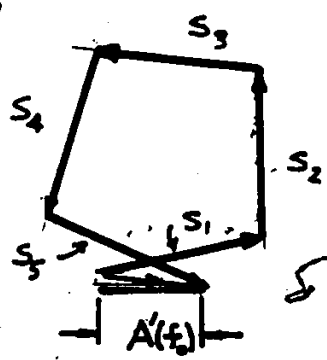
Figure 4.3(a) Phase summation of ideal delay line at harmonic frequency.

(b) Phase summation of unwanted harmonics.



$$Re[R(f)] = A'(f_s)$$

NOTE:  $A'(f) < A(f)$  FROM FIGURE 4.3 (a)



$$\phi_M = 10^\circ$$

- $S_1 \Rightarrow \underline{10^\circ + 10^\circ}$
- $S_2 \Rightarrow \underline{72^\circ + 20^\circ}$
- $S_3 \Rightarrow \underline{144^\circ + 30^\circ}$
- $S_4 \Rightarrow \underline{216^\circ + 40^\circ}$
- $S_5 \Rightarrow \underline{288^\circ + 50^\circ}$

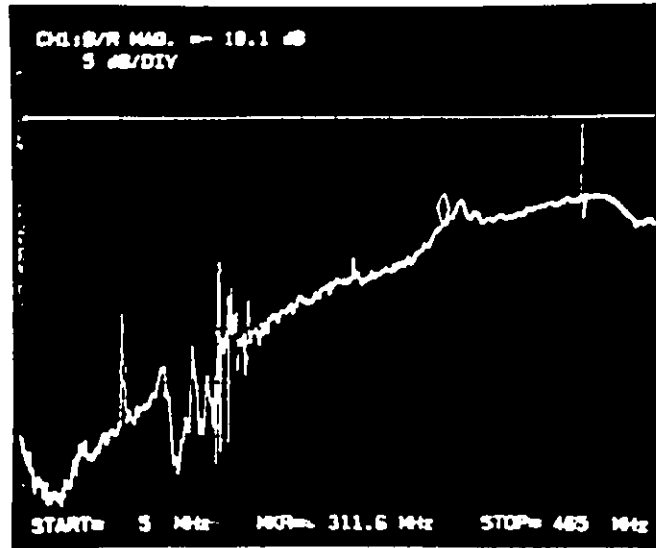
$$Re[R(f)] = A'(f)$$

(b)

Figure 4.4(a) Phase error interference at harmonic frequency.

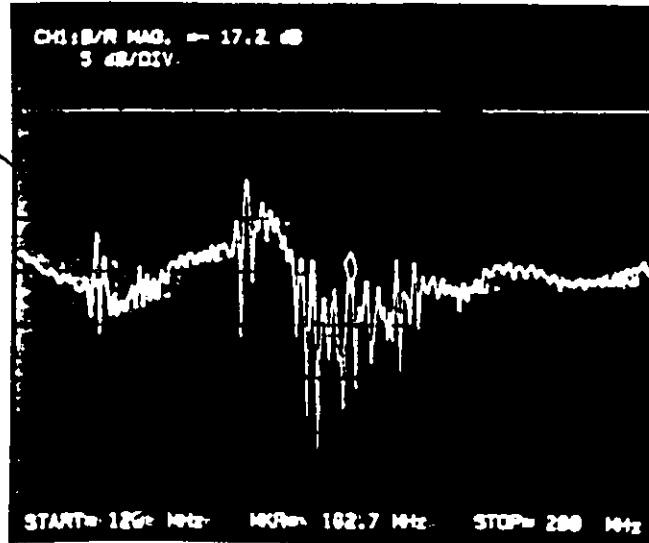
(b) Phase error interference at unwanted harmonic frequency.

-20 dB —  
(ref.)



(a)

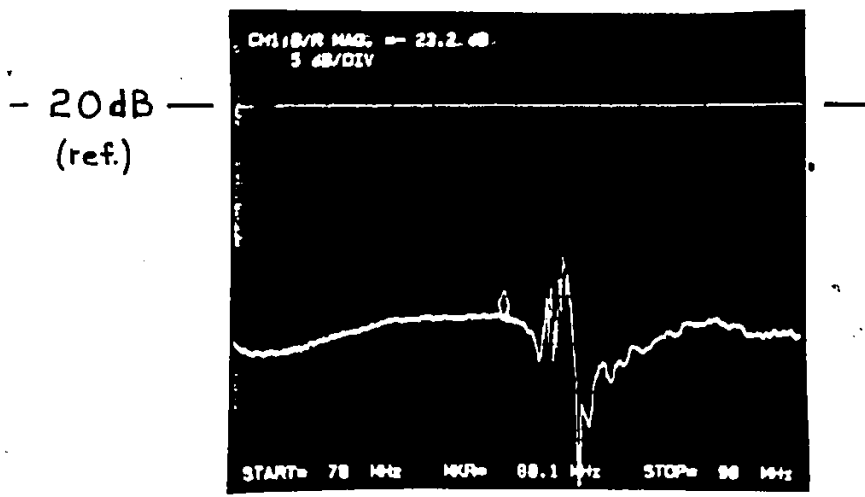
-30 dB —  
(ref.)



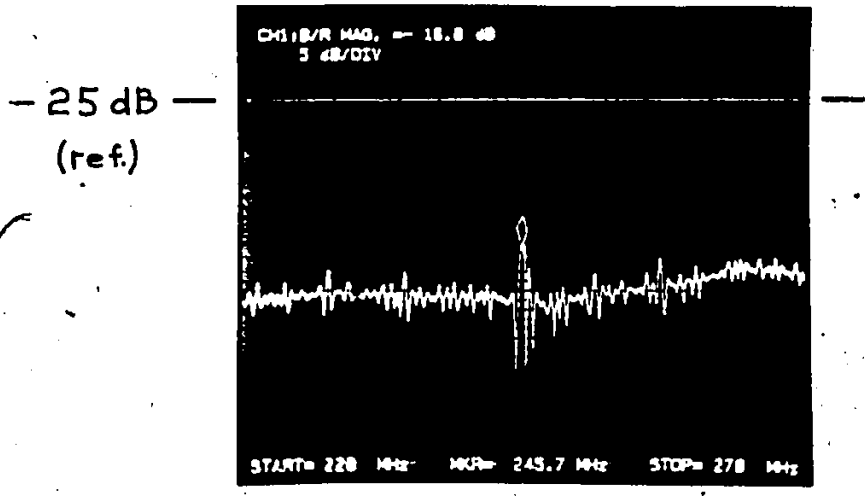
(b)

Figure 4.5(a) Frequency response of stepped-delay line.

(b) Bulk waves generated.



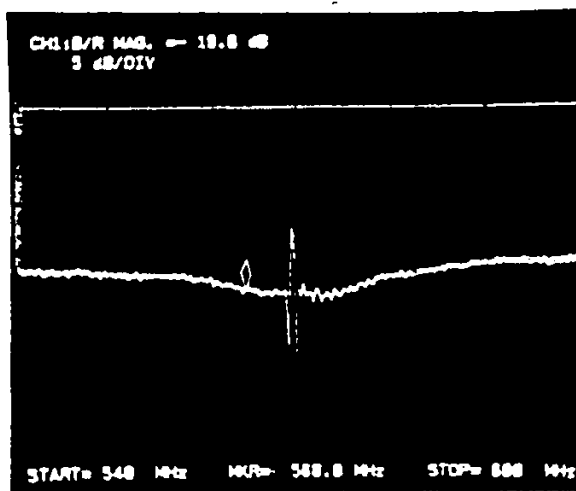
(a)



(b)

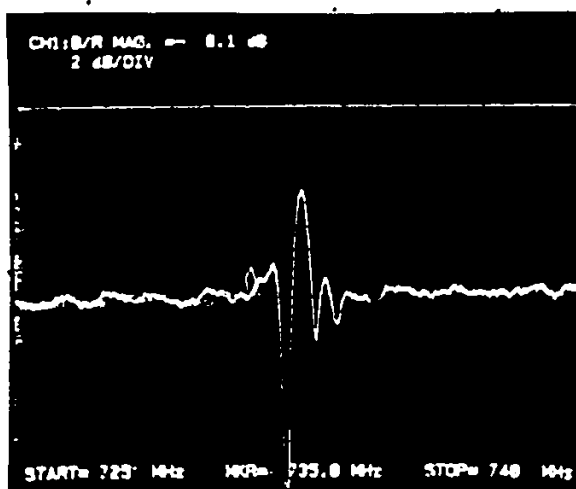
Figure 4.6 (a) Photograph of fundamental harmonic frequency.  
(b) Photograph of the 3rd harmonic frequency.

— 25 dB —  
(ref.)



(a)

— 40 dB —  
(ref.)

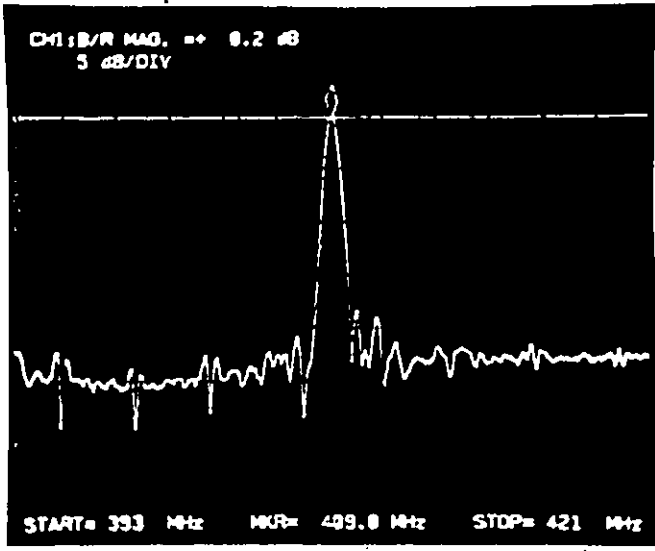


(b)

Figure 4.7(a) Photograph of the 7th harmonic frequency.

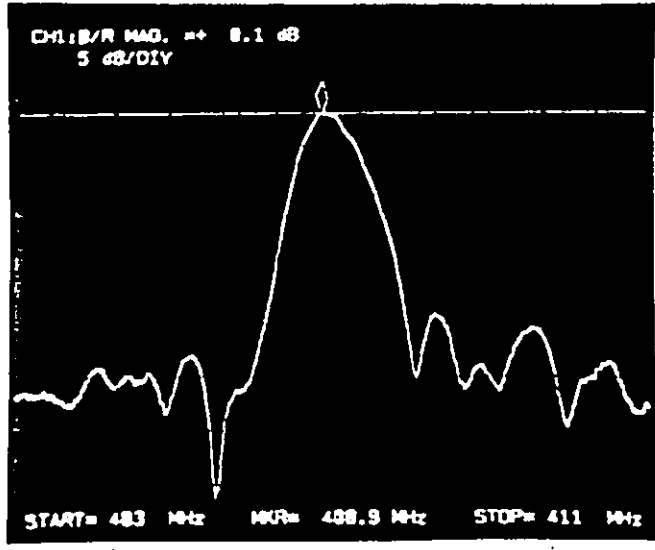
(b) Photograph of the 9th harmonic frequency.

0 dB  
(ref.)



(a)

0 dB  
(ref.)



(b)

Figure 4.8(a) Photograph of desired harmonic mode.

(b) Expanded view of the desired harmonic mode.



From examination of Figure 4.5(a) we note that the fundamental frequency is 18 dB down from the fifth harmonic frequency (i.e. fundamental frequency is at -38 dB from zero reference). The bulk wave interference was considerably reduced as shown in Figure 4.5(b).

Figure 4.6(a) gives an expanded view of the fundamental frequency. With the amplitude level of the fundamental 18 dB lower than the fifth harmonic frequency, the stepped finger delay line designed was a success for suppressing unwanted harmonic frequencies. Further evidence of this statement is illustrated in Figures 4.7 and 4.8. The relative amplitude response of the 3rd and 7th harmonic are theoretically zero (see Figure 3.2) when using a metallization ratio of  $n = 0.5$ . This is illustrated in Figures 4.6(b) showing the 3rd harmonic suppressed -40 dB and in Figure 4.7(a) showing the 7th harmonic frequency suppressed -38 dB. The fundamental and 9th harmonic frequency, illustrated in Figure 4.7(b), is suppressed -43.5 dB (the fundamental was discussed above).

Figure 4.8(a) shows the frequency response of the delay line and amplifier package shown in Figure 3.9(b). In Figure 4.8(b) the marker is located at the center frequency. there is a shift in the actual center frequency from  $f_M = 407.67$  MHz to  $f_M = 408.9$  MHz. This represents about an error of less than 1% in the center frequency of the desired

harmonic. This error is due to two reasons. First, the mass of the metal fingers causes a mass loading effect on the surface of the substrate, secondly the fingers act as shorts to the piezoelectric field hence the velocity of the surface wave is reduced.

The insertion loss at the desired harmonic frequency was 21.3 dB. The gain of the amplifier at the same frequency was 21.4 dB; hence the overall result was a gain of +0.1 dB as illustrated in Figure 4.8(b). This was sufficient to satisfy the closed loop gain constraint on oscillators as described in section 2.2 above and given by (2.2.1). Referring to Figure 4.8(b) the sidelobe suppression was 19 dB down from the peak at the desired harmonic frequency. This value is in accordance with P. Naraine's [30] results using a stepped-finger delay line operating at  $f_M = 114$  MHz.

The input and output capacitance as measured by the meter were:

$$C_{T_1} = 8.5 \text{ pF}$$

$$C_{T_2} = 3.2 \text{ pF}$$

These values were within 10% of their calculated values. This implies that the aperture width of the delay line was close to the optimum width for minimum untuned insertion loss. One aspect of designing the delay line was

to purposely achieve an insertion loss (IL) in the range  $IL = 19 - 21$  dB so that the oscillator can be constructed under the same conditions as mentioned in section 2.2, concerning oscillation criteria.

Though the delay line was designed to have an  $IL = 20$  dB, mismatching was still a crucial constraint. Figure 4.9 illustrates the input and output impedance measurement where the marker is fixed at the center frequency. From inspection of Figure 4.9(a) the input impedance is within 15% of  $50 \Omega$ , which can be considered a reasonable match for SAW transducers operating at such a high frequency. The VSWR was also calculated, since the Hewlett Packard 8505A Network Analyser is capable of measuring return loss. The measured return loss was  $R = -11.2$  dB. Substituting into (4.1.1) the reflection coefficient becomes

$$\rho = 10^{R/20} \quad (4.4.1)$$

$$\rho = 10^{-11.2/20}$$

$$\rho = 0.334$$

Hence, the VSWR becomes

$$VSWR = \frac{1 + |\rho|}{1 - |\rho|} \quad (4.1.2)$$

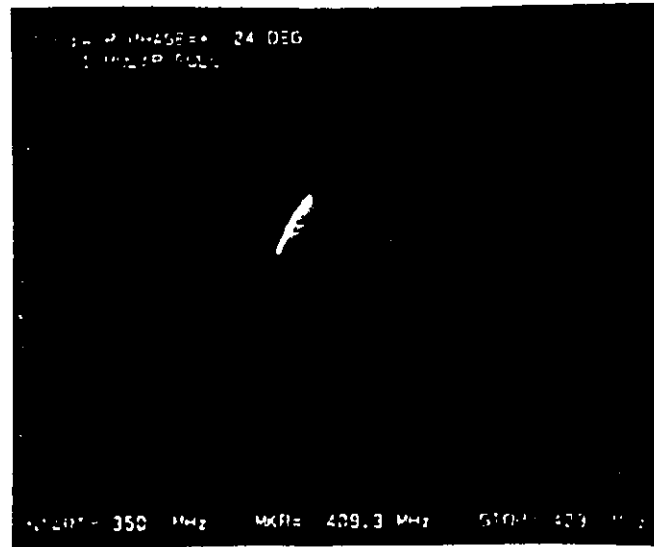
$$VSWR = 2.02$$

Having the  $VSWR = 2.02$  indicates a reasonable impedance matching circuit.

Figure 4.10(a) illustrates the phase of the delay line.



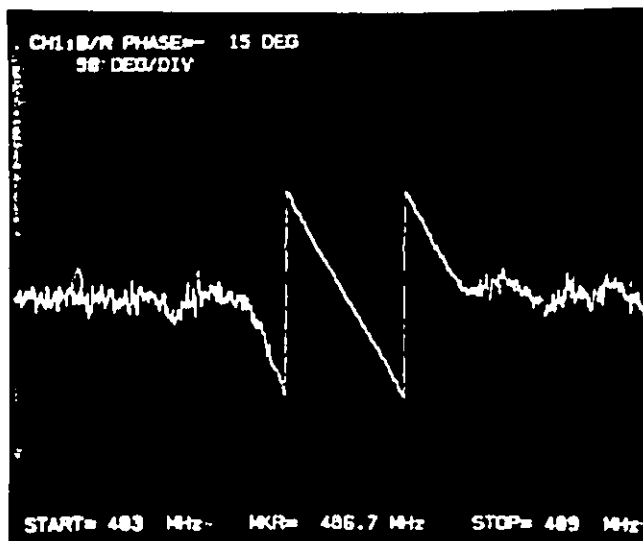
(a)



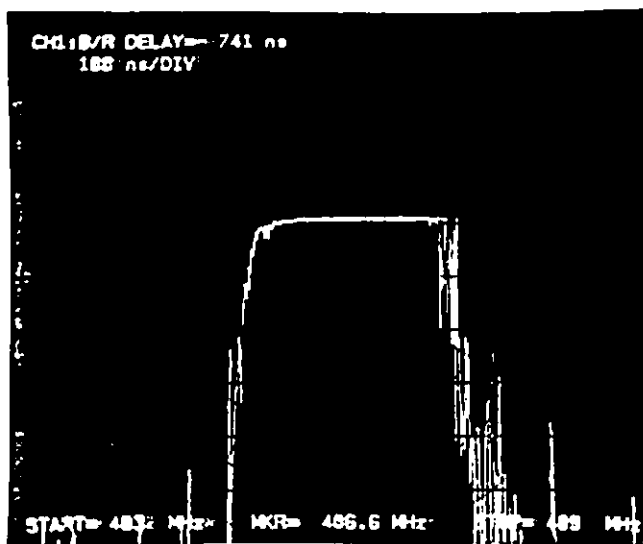
(b)

Figure 4.9(a) Photograph of the input impedance.

(b) Photograph of the output impedance.



(a)



(b)

Figure 4.10(a) Photograph of the phase response at desired harmonic frequency.

(b) Photograph of the group delay response at desired harmonic frequency.

The phase response appears to be linear as shown in the photograph. Figure 4.10(b) has information concerning the group delay line measurements. As shown in Figure 4.10(b), the group delay is less than 10 ns. Further investigation into phase and group delays are to be conducted by the author. By having a steep phase response the short term frequency stability can be improved since any fluctuation in the phase ( $\Delta\phi$ ) results in smaller fluctuations of the operation frequency ( $\Delta f$ ), as the steepness of the phase response increases.

From Figure 4.9(b) the null bandwidth was calculated to be

$$\Delta f_{\text{null points}} = 2.67 \text{ MHz}$$

$$f_{M_d} = 408.9 \text{ MHz}$$

therefore % BW = 0.6%. This value is approximately 50% from the theoretical value expected.

The Q-factor was calculated using the 3 dB points measured from the amplitude response (shown in Figure 4.9(b)). The result was a Q-factor of

$$\Delta f_{3dB} = 0.67 \text{ MHz}$$

$$f_o = 408.9 \text{ MHz}$$

$$Q = \frac{f_o}{\Delta f}$$

$$= \frac{480.9}{0.67}$$

$$Q = 610$$

The calculated Q-factor was 1229, resulting in an error of approximately 50%. This can be accounted for since there were a number of finger pairs broken during the fabrication process, hence reducing the theoretical Q-factor value.

#### 4.2 SAW Oscillator Results

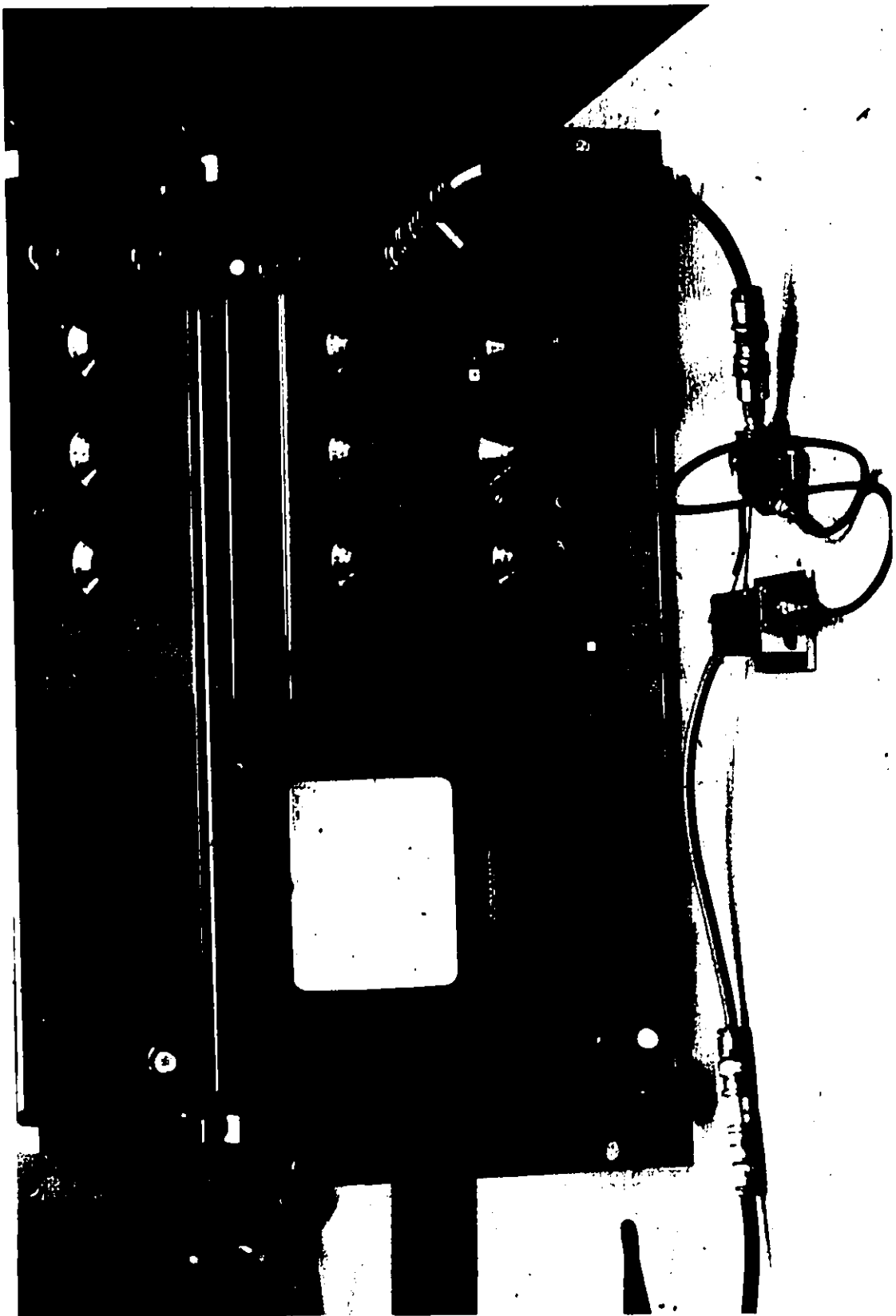
All spectrum measurements were obtained using a Hewlett Packard 855A Spectrum Analyzer. This configuration was chosen to view the closed-loop circuitry illustrated in Figure 3.11 because of the large dynamic range attainable (60-70 dB) in the amplitude response measurements. Figure 4.11 contains a photograph of the measuring system.

Figure 4.12(a) illustrates the spectrum of the oscillator output operating under closed-loop conditions, with the supply voltage set to 8.62 V. A second harmonic output appears at 810 MHz which is due to the amplifier's nonlinearity properties. The second harmonic is 25 dB down from the peak of the 5th harmonic frequency which is 10 dB down from the 0 dB reference. In Figure 4.12(b) an expanded view of the SAW oscillator's spectrum is illustrated operating at 404.3 MHz.

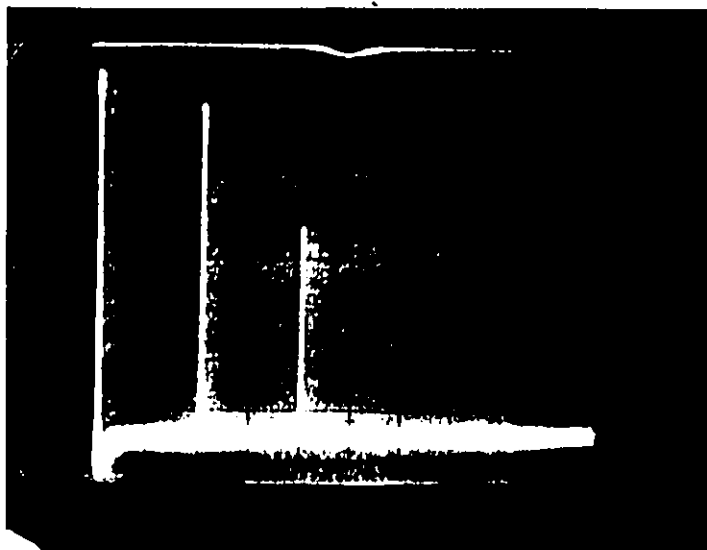
The output power is -15 dBm, with the supply voltage

Figure 4.11 Photograph of the Hp 8555A spectrum analyzer.





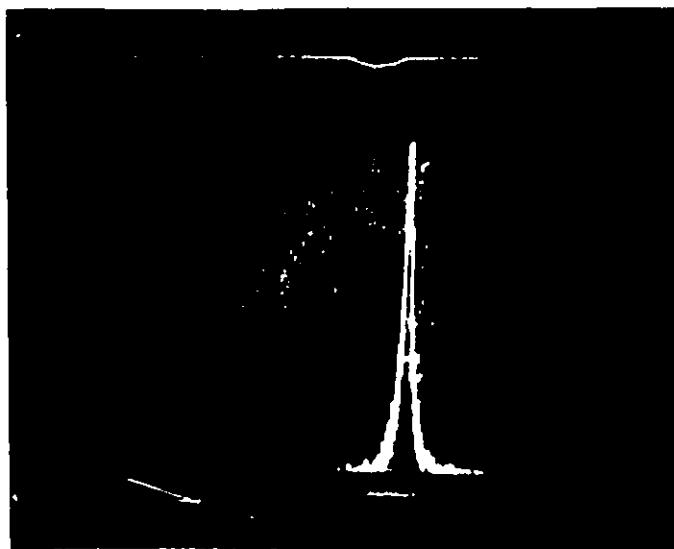
0 dBm  
(ref.)



(a)

404.808 MHz

0 dBm  
(ref.)



(b)

404.3 MHz

Figure 4.12(a) Spread spectrum of closed loop oscillator (illustrated amplifier).

(b) Spectrum of output oscillator.

set at 8.62 V.

A sketch of the short-term stability test set-up is illustrated in Figure 4.13. A photograph of this set up is shown in Figure 4.14.

The term short term stability in the time domain specifies the period fluctuations for intervals under 1 sec. The averaging times used in this thesis were  $T_a = 10^{-3}$ ,  $10^{-2}$ ,  $10^{-1}$ , and  $10^0$  seconds corresponding to a difference frequency of 1 kHz, 100 Hz, 10 Hz and 1 Hz, respectively.

The SAW oscillator output signal was fed to a power splitter (Merrimac PDM-20-500). From the power splitter half of the signal was then fed to a 50  $\Omega$  termination at the input to the frequency counter (HP 5340A), set to a 1 sec gate period, hence obtaining the average frequency over 1 sec with 1 Hz resolution. The time base of the counter was externally set by the synthesizer (HP Type 8660B) with a rated stability of  $\pm 3$  parts in  $10^8$  per 24 hours. The error introduced by the synthesizer (i.e. the reference oscillator) is so small that it may be ignored [28].

The other half of the power from the splitter is fed into a doubly balanced RF mixer (Merrimac DMM-2-250). The other input to the mixer comes from the synthesizer which is considered the local oscillator (LO). The frequency of the synthesizer is set by determining the average frequency of the oscillator under test, then setting the frequency

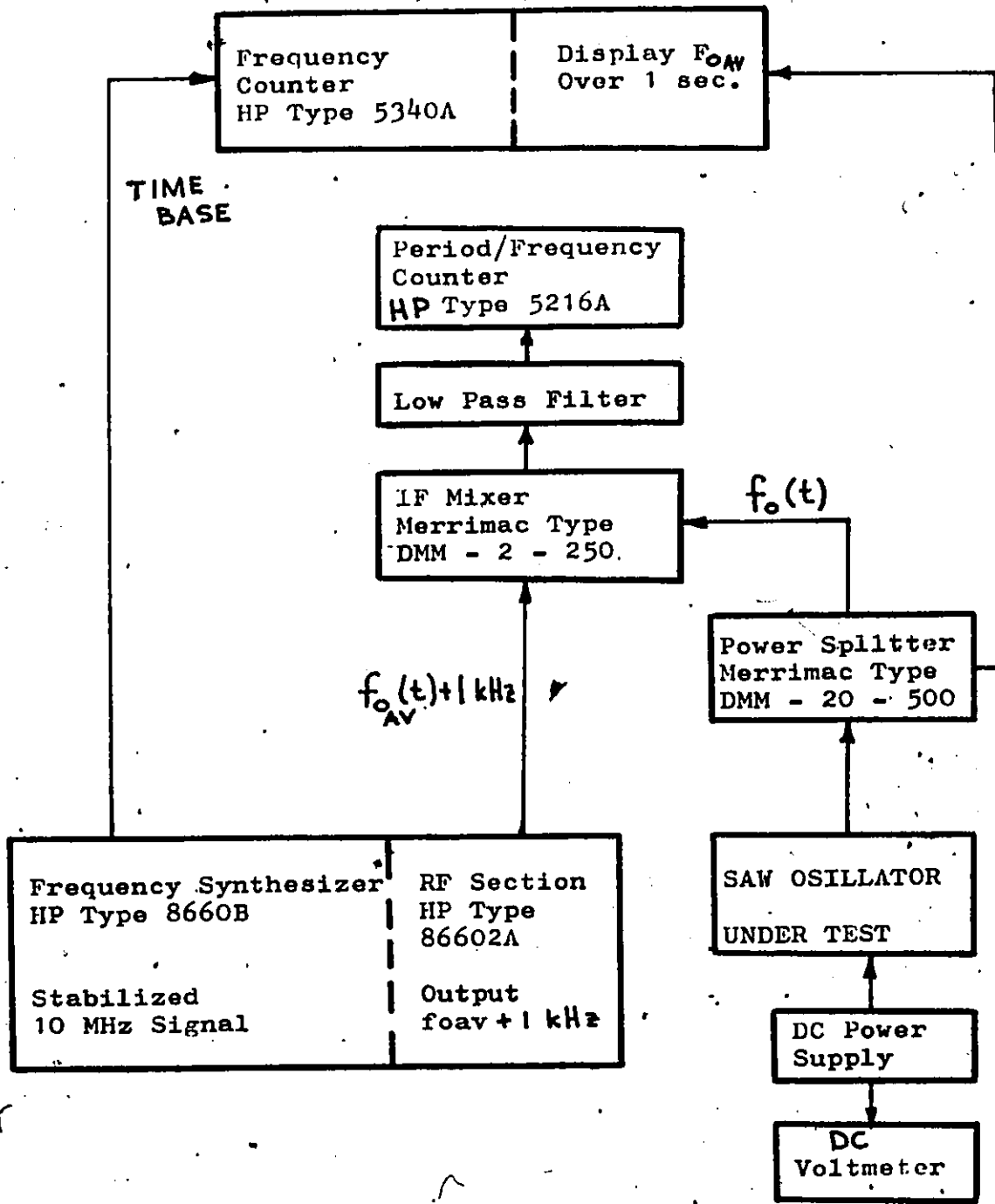
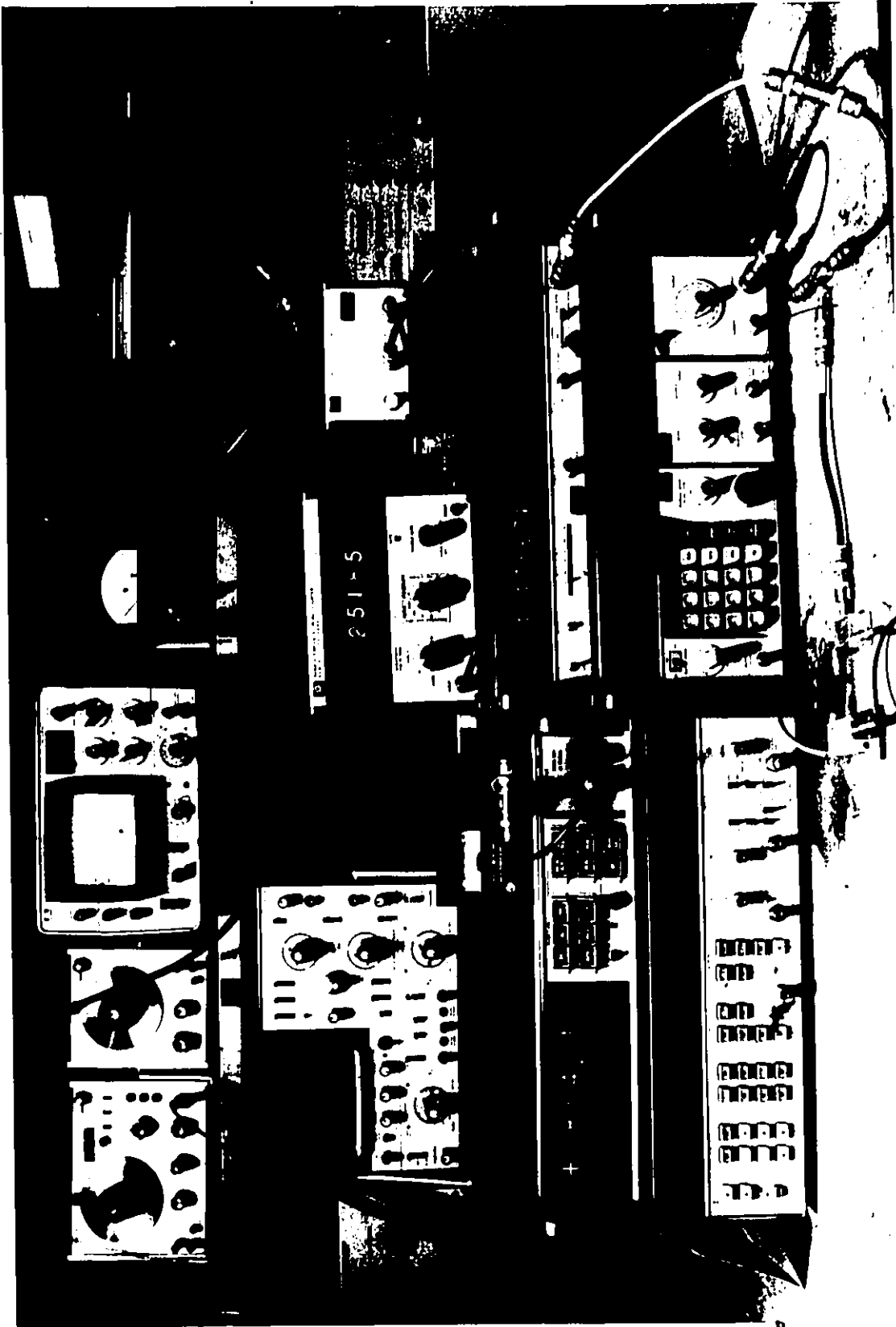


Figure 4.13 Block diagram of set up for short term stability measurements of SAW oscillators in time domain.

5  
Figure 4.14 Photograph of the test set for short term stability.



251-5

TELETYPE  
FERNET  
FERNET  
FERNET  
FERNET  
FERNET  
FERNET  
FERNET  
FERNET  
FERNET

synthesizer at a 1 kHz offset from the average SAW oscillator frequency, i.e.

$$f_S = f_{M_d \text{ AVE}} + 1 \text{ kHz}$$

The output from the mixer is the sum and difference frequencies

$$f_H = f_{M_d \text{ AVE}} + f_S \quad (4.2.1)$$

$$f_L = f_{M_d \text{ AVE}} - f_S \quad (4.2.2)$$

where  $f_H$  and  $f_L$  represent the sum and difference of the heterodyned frequencies. These signals are fed into a low pass filter, with  $f_{\text{CUTOFF}} = 12.5 \text{ MHz}$ , which removes  $f_H$  resulting in only the presence of  $f_L$ . Because the stability was conducted in the time domain the individual periods are counted. To display a count with 1 Hz resolution the gate time must be selected to 1 sec, similarly for 10 Hz results in a 0.1 sec gating time. Thus, for an average over 1 msec the frequency of the synthesizer becomes

$$f_S = f_{M_d \text{ ave}} + 1 \text{ kHz.}$$

A drift in the oscillator under test from the 1 kHz difference frequency will correspond to drifts from 1 msec period (see section 2.5.1). The statistical values required for short term stability in the time domain as described in section 2.5.1 are, the mean period  $\tau$ , the standard deviation of the period  $\Delta\tau$ , and the mean frequency  $f_M$ . To calculate

the mean (4.4.3) was used

$$f_{MN} = \frac{1}{N} \sum_{n=1}^N \left( \frac{1}{T_n} \right) \quad (4.4.3)$$

where  $T_n$  is the period for the average difference frequency (average value over 100 samples was used), i.e.

$$T_n = \frac{1}{|f_{M_d \text{ AVE}} - f_{SAW}(t)|} \quad (4.4.4)$$

Furthermore, the standard deviation becomes

$$\sigma = \text{standard deviation} = \sqrt{\frac{1}{N-1} \sum_{n=1}^N \left( \left| \frac{1}{T_n} - f_{MN} \right| \right)^2}$$

For periods longer than 1 msec the same configuration was used but only 10 periods were counted, as opposed to the 100 periods counted at 1 msec, with the difference frequency still at 1 kHz. The results for the SAW oscillator are listed in Table IV.



TABLE IV

Short term stability of the 404.367 MHz SAW Oscillator

| Averaging Time | Mean Period    | Standard Deviation of Period | Mean Frequency  | Short Term Stability    |
|----------------|----------------|------------------------------|-----------------|-------------------------|
| 1 [msec]       | 1.030 [msec]   | 0.01145 [msec]               | 404.36720 [MHz] | 2.67 parts in $10^8$    |
| 10 [msec]      | 10.135 [msec]  | 0.05482 [msec]               | 404.36720 [MHz] | 1.32 parts in $10^9$    |
| 100 [msec]     | 100.648 [msec] | 2.59702 [msec]               | 404.36721 [MHz] | 6.34 parts in $10^{10}$ |
| 1 [sec]        | 1.070 [sec]    | 120.832 [msec]               | 404.36752 [MHz] | 2.61 parts in $10^{10}$ |

## CHAPTER V

### CONCLUSIONS AND RECOMMENDATIONS

Previous SAW interdigital transducer circuitry fabricated at McMaster University with the aid of photolithographic techniques have been limited to an upper bound of 185 MHz. With the use of the stepped-finger delay line, higher harmonic operating frequencies can be obtained while the fabrication technique depend on the fundamental frequency.

The performance of the harmonic delay lines when used as a feedback element in a SAW oscillator has proven to be successful. The short term stability values and the power outputs are all compatible with the present manufactured SAW oscillators by Plessey Semiconductors [38]. Hence, it is possible by utilizing the higher spatial harmonics, to substantially ease the fabrication of SAW oscillators in the UHF/VHF region.

A description was given of a design technique for the SAW oscillator construction. Though delay lines operating at harmonic models provide a larger frequency range in which to operate, the resonator must still be considered, since it exhibits better overall performance mainly due to the higher achievable Q-factors.

Improvements to the delay line-type oscillator relate to improvements of the amplifier circuitry. Future improvements are expected when a pin diode circuitry prior to the amplifier input is used. (Such methods are being considered for investigation at McMaster.)

## REFERENCES

1. Farnell, G.W., "Elastic Surface Waves", H. Mathews, (ed.), Surface Wave Filters, New York: Wiley, 1977, Ch. 1.
2. Vallers, H.G. and Clairborne, L.T., "RF Oscillator Control Utilizing Surface Wave Delay Lines", Proceedings of the 28th Annual Frequency Control Symposium, Atlantic City, p. 266-269, May 1974.
3. Laurence, M.W., "Surface Acoustic Wave Oscillators", J.H. Collins (Ed.), Computer-aided Design of Surface Acoustic Wave Devices, Elsevier Scientific; Amsterdam, 1976, Ch. 8.
4. Crabb, J., Lewis, M., and Maines, J.D., "Surface Acoustic Wave Oscillators: Mode Selection and Frequency Modulation", Electronics Letters, Vol. 9, No. 10, p. 193, May 1973.
5. Karren, H. and Dias, J.F., "Surface Acoustic Wave Oscillators", Proceedings of the 29th Annual Frequency Symposium, Atlantic City, p. 266-269, May 1974.
6. Hartmann, C.S., Bell, D.T. and Rosenfeld, R.C., "Impulse Model design of Acoustic Surface Wave Filters", IEEE MTT-21, No. 4, p. 162-175, April 1973.
7. Smith, W.R., "Key Tradeoffs in SAW Transducer Design and Component Specification", Proc. 1976 IEEE Ultrasonic Symposium, pp. 547-552.
8. Lewis, M.F., "Some Aspects of SAW Oscillators", Proc. on Sonic and Ultrasonic Symposium, Monterey, California, p. 508-511, Sept. 1973.
9. Staples, E.J., "UHF Surface Acoustic Waves", Proc. of the 28th Annual Frequency Control Symposium, Atlantic City, p. 280-285, May 1974.
10. Williamson, R.C., "Reflecting Grating Filters", H. Mathews, (Ed.), Surface Wave Filters, New York, Wiley, 1977, Ch. 9.
11. Oliner, A., Bertoni, H., Li, R.M., "Catalog of Acoustic Equivalent Networks for Planar Interface", Proc. IEEE, Vol. 60, p. 1503-1520, May 1972.

12. Lewis, M.F., Bale, R., "Improvements to SAW Oscillators", Proc. 1974 Ultrasonic Symposium, IEEE Publication 74 CH08961SU, p. 272-275, , 1974.
13. Parker, T.E. and Lee, D.L., "Stability on Phase Shift on Quartz SAW Devices", Proc. of the 33rd Annual Frequency Control Symposium, Atlantic City, p. 379-387, May 1974.
14. Seiler, D.G., "Design and Synthesis of a UHF Surface Acoustic Wave Oscillator", M,Eng. Thesis, McMaster University, Dec. 1975.
15. Hodur, E.P., "A Designer's File: Notes on SAW Bandpass Filters", Microwave Journal, p. 72-76, Oct. 1980.
16. Li, R.C., Alusow, J.A. and Williamson, R.C., "Experimental Exploration of the Limits of Achievable Q of Grooved Surface-Wave Resonators", Proc. 1974 Ultrasonics Symposium, New York, IEEE Publication 74 CH1240-55U, p. 245-252, Sept. 1974.
17. Dolochychi, S.J., Staples, E.J., White, J. and Lim, T.C., "Hybrid SAW Oscillator Fabrication and Packaging", Proc. of the 32nd Annual Frequency Control Symposium, Atlantic City, p. 385-394, May 1979.
18. Staples, E.J. and T.c. Lim, "300 MHz Oscillator using Resonators and Delay Lines", Proc. of the 31st Annual Frequency Control Symposium; Atlantic City, p. 371-374, May 1977.
19. Parker, T.E., "Current Developments in SAW Oscillator Stability", Proc. of the 31st Annual Frequency Control Symposium, Atlantic City, p. 359-362, May 1977.
20. Leeson, D.F., "Short Term Stable Microwave Sources", Microwave Journal, p. 59-69, June 1970.
21. Williamson, J., Farr, A.N., Gratze, S.C. and Slater, J., "Some Recent Developments in Surface Acoustic Wave Oscillators", The Marconi Review, second quarter, p. 86-115, June 1980.
22. Lance, A.L., Seal, W.D., Mendoza, J.G. and Hudson, N.W., "Automating Phase Noise Measurements in the Frequency Domain", Proc. of the 31st Annual Frequency Control Symposium, Atlantic City, p. 357-358, May 1977.

23. Campbell, C.K., "Observation on the Short Term Stability of a SAW Delay Line Oscillator", Proc. 1980 Ultrasonic Symposium, Boston, IEEE Publication 80 CH1602-2, p. 260-263, Oct. 1980.
24. Osterdock, T., "Timekeeping and Frequency Calibration", Hewlett Packard Application, Note 52-2, June 1974.
25. Leeson, D.B., "A Simple Model of Feedback Oscillator Noise Spectrum", Proc. IEEE, Vol. 54, p. 329-330, Feb. 1966.
26. Parker, T.E. and Shulz, M.B., "Temperature Stable Surface Acoustic Wave Delay Lines with SiO<sub>2</sub> Film Overlays", Proc. 1974 Ultrasonic Symposium, p. 295-299, Nov. 1974.
27. Lewis, M., "The Surface Acoustic Wave Oscillator - A Natural and Timely Development of the Quartz Crystal Oscillator", Proc. of the 28th Annual Frequency Control Symposium, Atlantic City, p. 304-314, May 1974.
28. Campbell, C.K., "A Feasibility Study of VHF/UHF Surface Acoustic Wave (SAW) Oscillators", Communication Research Laboratory, McMaster University, Dec. 1977.
29. Penunuri, D. and Lakin, K.M., "Surface Acoustic Wave Velocities of Isotropic Metal Films on Selected cuts of Bi<sub>12</sub>GO<sub>20</sub> Quartz, Al<sub>2</sub>O<sub>3</sub> and LiNbO<sub>3</sub>", IEEE Trans. on Sonic and Ultrasonics, SU-21, Vol. 4, p. 293-295, 1974.
30. Naraine, P.M., "Design and Synthesis of Harmonic Surface Acoustic Wave Delay Lines", CRL Internal Report Series, McMaster University, No. CRL-83, Sept. 1980.
31. Shulz, M. and Holland, M., "Surface Acoustic Wave Delay Lines with Small Temperature Coefficients", Proc. of IEEE, p. 1361-1362, Sept. 1970.
32. Shultz, M. and Holland, M., "Materials for Surface Acoustic Wave Devices", IEEE Seminar on Components Performance and Systems Applications of Surface Acoustic Wave Devices, p. 1-10, Sept. 1973.
33. Kerbel, S., "Design of Harmonic Surface Acoustic Wave (SAW) Oscillators without External Filtering and New Data on the Temperature Coefficient of the Quartz", Proc. of the IEEE, Proc. 1974 Ultrasonic Symposium, p. 276-281, 1974.

34. Shoalf, J.H., Halford, D. and Risley, A., "Frequency Stability Specifications and Measurements: High Frequency and Microwave Signals", NBS Technical Report 632, U.S. Department of Commerce/National Bureau of Standards, January 1973.
35. Barnes, J.A., "Characterization of Frequency Stability", IEEE Trans. on Instrumentation and Measurement, Vol. IM-20, No. 2, p. 105-120, May 1971.
36. "Understanding and Measuring Phase Noise in the Frequency Domain", Application Note 207, Hewlett Packard Co., October 1976.
37. Milson, R.F., "Bulk Wave Generation by the IDT", J. Collins (Ed.), Computer Aided-Design of Surface Acoustic Wave Devices, Elsevier Scientific, Amsterdam, 1976, Ch. 5.
38. "Provincial Data", Publication Note 2129, Issue No. 1-875, Plessey Semiconductor Co., 1980.
39. Naraine, P., Campbell, C.K., Y. Ye, "A SAW Step-type Delay Line for Efficient High Order Harmonic Mode Excitation", Proc. 1980 Ultrasonic Symposium, Boston, IEEE Publication No. 80CH1602-2, p. 322-325, Oct. 1980.

## APPENDIX A

### PHASE NOISE

Phase noise is the term used to describe the characteristic randomness of frequency. The term spectral purity refers to the signal power to phase noise sideband power ratio. Spurious signals are outputs in the spectrum of a source that are neither part of the carrier nor its harmonics, and they may be discrete frequencies or bands of frequencies. The spectral content of the noise modulating signals is finite in bandwidth and does not have the same bandwidth and same amplitude at all frequencies as one finds with white noise.

Practical oscillators demonstrate noise which appears to be a combination of generated signals and random, non-deterministic noises. The random noises include thermal noise, shot noise and noise of undetermined origin (such as flicker noise). These result in time dependent phase and amplitude fluctuations of the signal.

To clarify the definition of phase noise and its relationship to frequency stability, a brief summary of the theoretical work of the U.S. National Bureau of Standards, [34] will be presented.

The instantaneous output voltage  $V(t)$  of an oscillator



may be written as [35]

$$V(t) = [V_0 + \epsilon(t)] \sin(2\pi f_0 t + \phi(t)) \quad (A-1)$$

where  $V_0$  and  $f_0$  are the operating amplitude and frequency,  $\epsilon(t)$  and  $\phi(t)$  are the instantaneous amplitude and phase fluctuations.

The instantaneous angular frequency  $\omega(t)$  is defined as [35]

$$\omega(t) = \frac{d}{dt} (2\pi f_0 t + \phi(t))$$

$$\omega(t) = 2\pi f_0 + \frac{d}{dt} \phi(t)$$

$$\omega(t) = 2\pi f_0 + \dot{\phi}(t) \quad (A-2)$$

where

$$\dot{\phi}(t) = \frac{d}{dt} \phi(t) \quad (A-3)$$

Both  $\phi(t)$  and  $\dot{\phi}(t)$  are assumed to be zero mean and a stationary random process [35]. Rearranging (A-2)

$$\dot{\phi}(t) = 2\pi (f(t) - f_0)$$

$$\dot{\phi}(t) = 2\pi \Delta f(t) \quad (A-4)$$

Dividing both sides of (A-4) by  $f_0$  and rearranging terms,

$$\frac{\Delta f(t)}{f_0} = \frac{\dot{\phi}(t)}{2\pi f_0} \quad (A-5)$$

where

$$\frac{\Delta f(t)}{f_0}$$

represents the instantaneous fractional frequency deviation

(define  $y = \Delta f(t)/f_0$ ) from the nominal frequency  $f_0$ .

Since  $\phi(t)$  is a stationary process, it is differentiable in the mean square sense if its correlation function  $R_\phi(\tau)$  has derivatives of the order up to two, i.e.

$$R_\phi(\tau) = \int_{-\infty}^{\infty} \dot{\phi}(t) \dot{\phi}(t+\tau) dt \quad (\text{A-6})$$

Let

$$u = \dot{\phi}(t+\tau)$$

and

$$dv = \dot{\phi}(t) dt$$

so that

$$du = \ddot{\phi}(t+\tau)$$

and

$$v = \phi(t)$$

substituting into (A-6)

$$R_\phi(\tau) = \dot{\phi}(t+\tau) \phi(t) - \int_{-\infty}^{\infty} \phi(t) \ddot{\phi}(t+\tau) dt \quad (\text{A-7})$$

which reduces to (A-8)

$$R_\phi(\tau) = - \int_{-\infty}^{\infty} \phi(t) \ddot{\phi}(t+\tau) dt \quad (\text{A-8})$$

From definition

$$\begin{aligned} \ddot{\phi}(t+\tau) &= \frac{d^2}{d(t+\tau)^2} \phi(t+\tau) \\ &= \frac{d^2}{d\tau^2} \phi(t+\tau) \end{aligned}$$

Hence (A-8) becomes

$$R_{\phi}^*(\tau) = - \frac{d^2}{d\tau^2} \int_{-\infty}^{\infty} \phi(t) \phi(t+\tau) dt \quad (A-9)$$

The autocorrelation function of  $\phi(t)$  is defined as

$$R_{\phi}(\tau) = \int_{-\infty}^{\infty} \phi(t) \phi(t+\tau) dt$$

Hence (A-9) reduces to

$$R_{\phi}^*(\tau) = - \frac{d^2}{d\tau^2} R_{\phi}(\tau) \quad (A-10)$$

Hence, taking the Fourier transform of the correlation function,

$$S_{\phi}^*(f) \Rightarrow R_{\phi}^*(\tau) \quad (A-11)$$

Since  $\phi(t)$  exists and is stationary, it is possible to consider the following spectral densities,  $S_{\phi}(f)$ ,  $S_{\Delta f}(f)$  and  $S_Y(f)$  [35].

$S_Y(f)$  defines the spectral density of fractional frequency fluctuations on a per hertz basis,

$$S_Y(f) = \left(\frac{1}{f_0}\right)^2 S_{\Delta f}(f) \left[\frac{1}{\text{Hz}}\right] \quad (A-12)$$

$S_{\Delta f}(f)$  is the one-sided spectral density of frequency fluctuations  $\Delta f$ . It is defined as,

$$S_{\Delta f}(f) = \frac{(\Delta f_{\text{rms}})^2}{(\text{Bandwidth used in the measurement of } \Delta f_{\text{rms}})} \left[\frac{\text{Hz}^2}{\text{Hz}}\right] \quad (A-13)$$

$S_{\phi}(f)$  is the one-sided spectral density of the phase

fluctuations which is defined as

$$S_{\phi}(f) = \frac{S_{V_{rms}}(f)}{K^2} \left[ \frac{\text{rad}^2}{\text{Hz}} \right] \quad (\text{A-14})$$

where

$S_{V_{rms}}(f)$  is the power spectral density of the voltage fluctuation out of the phase detector,

$K$  is the phase detector constant (volts/radians)

The U.S. National Bureau of Standards [34] recommends that the spectral density of the instantaneous frequency fluctuations,  $S_y(f)$ , be used as the primary definition of frequency stability in the frequency domain. Hence,  $S_y(f)$  can be related to  $S_{\phi}(f)$  as from (A-12)

$$S_y(f) = \left( \frac{1}{f_0} \right)^2 S_{\Delta f}$$

Also from (A-10) and (A-11)

$$S_{\Delta f}(f) = 2\pi^2 f^2 S_{\phi}(f) \quad (\text{A-15})$$

From reference [35]

$$S_{\Delta f}(f) = f^2 S_{\phi}(f) \quad (\text{A-16})$$

substituting (A-16) into (A-12)

$$S_y(f) = \left( \frac{f}{f_0} \right)^2 S_{\phi}(f) \left[ \frac{1}{\text{Hz}} \right] \quad (\text{A-17})$$

A useful measure of frequency stability relates the sideband power associated with phase fluctuations to the carrier power level. The defined measure is called Script  $\mathcal{L}(f)$  and is the ratio of the power per hertz of bandwidth at

frequency  $f$  from the carrier in one phase noise sideband to the carrier power, (see equation 2.5.3). From small angle modulation theory [35]

$$\text{Script } \mathcal{L}(f) = 10 \log_{10} \left[ \frac{S_{\phi}(f)}{2} \right] \left[ \frac{\text{dB}}{\text{Hz}} \right] (1 \text{ Hz BW}) \quad (\text{A-18})$$

Note, that the theory, definitions and equations given above relate to only one device.

## APPENDIX B

### INSERTION LOSS EQUATIONS FOR DELAY LINE AND RESONATOR

For the delay line [20],

IL  $\propto$   $\tau$  (the insertion loss increases linearly with  $\tau$ ).

$$\tau = \frac{8.69}{\alpha}$$

where  $\alpha$  = the propagation loss

IL = the insertion loss.

For the resonator [26],

$$IL_{(dB)} = 10 \log_{10} \left( \frac{1}{1 - \frac{QL}{Qu}} \right)$$

which reduces to [20]

$$\tau = \frac{2QL}{f_0}$$

Hence, the IL for the resonators can be minimized to the unloaded Q of the material which gives an insertion loss of about 5 dB. The typical delay line has an untuned insertion loss of IL  $\approx$  14 - 25 dB. This is not according to the theoretical value because of propagation loss and bidirectionality loss of the transducer (i.e. this accounts for 6 dB).

APPENDIX C  
PACKAGING CONSIDERATIONS

The important factors to be considered in the design of a package to house the SAW oscillator, are mechanical, environmental and electrical.

The case can be a metal box with a milled cavity, a stripline configuration or a combination of both metal box and stripline. The most common case used is a metal I-beam frame, which contains the substrate on one side and the electrical components (matching networks, amplifiers, etc.) on the other side. The case is usually insulated with soft foam shroud to protect the crystal from damage when subjected to shock and vibration. The transducers are connected to the matching networks via an insulated mechanical feedthrough.

The crystal substrate must be securely fastened to the housing. The mounting and bonding techniques used must allow the crystal substrate to be firmly bonded and also provide a cushioning effect. In general, the RTV adhesives are used to attach the substrate to the package frame. RTV cures at room temperature to a soft plastic state. This allows the substrate to be firmly held in place while permitting it to float on a layer of RTV.

The method adopted at the SAW laboratory at McMaster University is mount crystals, using apiezon grease on the bottom side of the crystal substrate. An even layer of about 40 mil is applied to the backside, then the substrate is placed into position and pressure is gently applied to the edges of the substrate until it seats permanently in the layer of grease. The grease also is used to absorb the bulk waves at the bottom of the substrate. Removal of a substrate, mounted with RTV is more difficult than that mounted with grease. The grease dissolves in trichloroethylene, which does not damage the substrate, whereas with RTV, a thin wire must be used to cut through the layer of RTV to remove the substrate.

Moisture and particulate matter such as dirt and dust are undesirable elements on the crystal surface. Aluminum transducers used on quartz and  $\text{LiNbO}_3$  oxidize in the presence of moisture. Oxidation changes the sheet resistivity of the electrodes and creates pinholes in the transducers that alter the transducer impedance. Hence, moisture will adversely affect the yield, performance, aging and reliability of the sealed hybrid enclosure. Failure modes associated with moisture include parameter drifts, wire bond and metallization corrosion.

The most commonly used method to remove moisture is to control the internal package condition. Packages are placed



in a vacuum oven for 8 hours to bake off as much moisture as possible. Then the package is transferred through a moisture monitored  $N_2$  atmosphere to the weld chamber where the unit is evacuated to  $2 \times 10^{-7}$  Torr and resistive welding is completed.

Electromagnetic feedthrough in SAW filters is defined as the energy that is electrically coupled or radiated from one transducer to the other. Electromagnetic suppression is the ratio of the amount of electromagnetic feedthrough to the output acoustic response level. Usually the two summing bars of the transducer are connected to an unbalanced transmission line with gold wires. In this arrangement, one side of the transducer is grounded to the metal box housing the substrate, while the other is connected to the  $50 \Omega$  input terminal. The result is that unbalanced feed arrangement behaves as a guided wave phenomena. This type of feed results in the generation of normal E-field components that tend to excite modes in the waveguide. These modes give rise to electromagnetic feedthrough when the distance between the transducers is small, see Figure C-1.

To remove electromagnetic feedthrough short transducers should be used since they do not radiate electromagnetically as strongly as do long transducers. The effective height of the cavity should be made nearly equal to the height of the crystal.

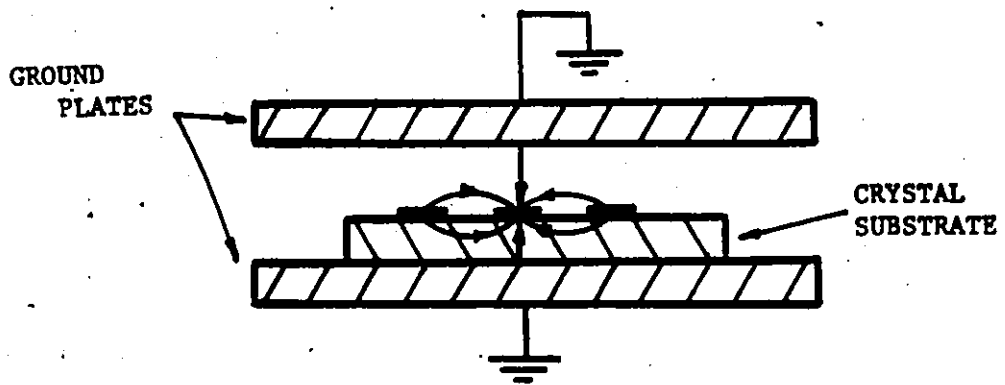
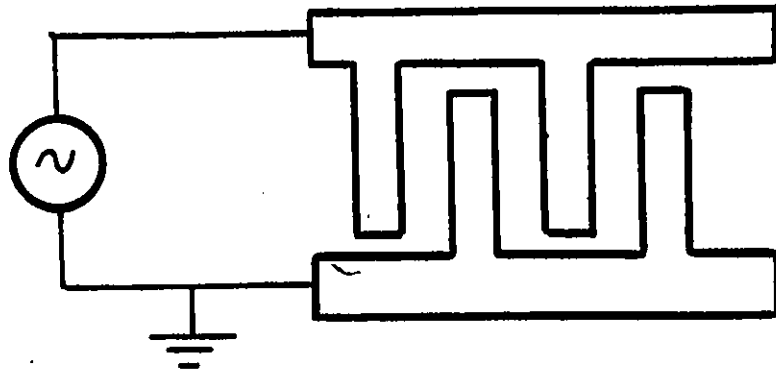


Figure C-1 Electrical field diagram of unbalanced connection.

Another solution to remove the TE-mode excited in the cavity is to use a balanced transformer. As shown in Figure C-2, with a balanced transformer, there is no net normal E-field, thus the TE-modes are suppressed, which implies that the electromagnetic interaction of the transducers will be eliminated.

The thermal environment of the crystal substrate must be controlled since any changes in temperature of the SAW filter result in changes in the operating frequency due to velocity variations, gain in the amplifier and substrate dimensions. Package ovens and heaters are generally used but they have two major disadvantages. First, the package ovens are large hence pose a problem when spacing is a constraint; second, it is difficult to place semiconductor electronics inside the package ovens.

The feedstructure is defined as the physical network from which the electrical signal is launched to a transducer on a crystal substrate. Short transducers have small electrode capacitance, thus the feedstructure must have minimum parasitic capacitance, to reduce insertion loss. At high frequencies ( $f > 200$  MHz) the terminal points should be mounted as close to the transducers as possible to minimize the series inductance associated with the gold wire.

The metal thickness of the transducer is in the order of 500 to 5000 Å. Conventional wire soldering or gap

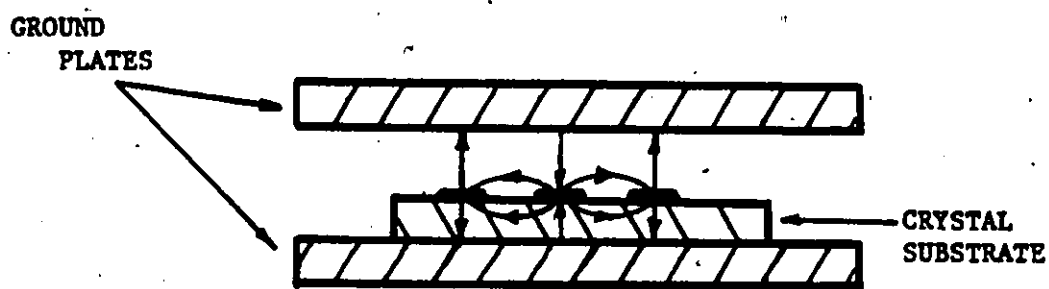
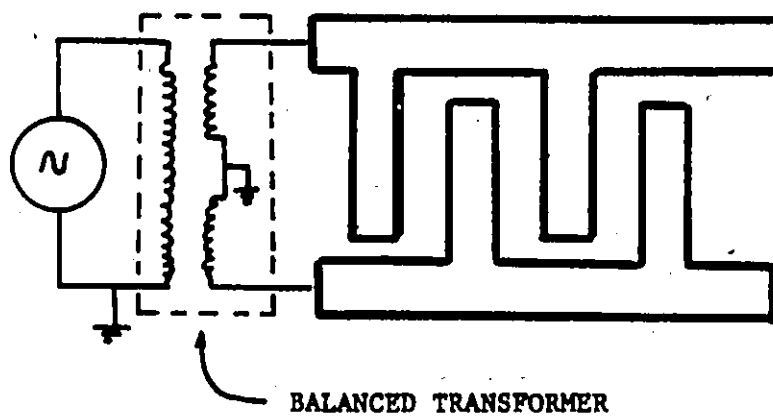


Figure C-2 Electrical field diagram of balanced connection.

welding is not appropriate here, instead methods of connecting the feed structures are by ultrasonic and thermocompression wire bonding. The ultrasonic wire bonder attaches aluminum or gold wires using pressure and ultrasonic energy that converts to heat. The disadvantage is that ultrasonic forces can easily crack the crystal if not properly mounted in the package. The thermocompression wire bonder attaches only gold wire using heat and pressure. This method is more reliable to use, since heat is delivered through a capillary as a heat stage.